IN THE UNITED STATES DISTRICT COURT

FOR THE DISTRICT OF DELAWARE

ZYMOGENETICS, INC., a Washington Corporation, Plaintiff, v. BRISTOL-MYERS SQUIBB CO., a Delaware Corporation, and DOES 1 through 100, Defendants.	)	C.A. No. 06-500-SLR **PUBLIC VERSION**

DECLARATION OF PAUL J. ANDRE IN SUPPORT OF ZYMOGENETICS, INC.'S MOTION FOR SUMMARY JUDGMENT OF INFRINGEMENT OF THE PATENTS-IN-SUIT

Volume 2 of 2

Exhibits 9 - 18

Philip A. Rovner (#3215)
POTTER ANDERSON & CORROON LLP
Hercules Plaza
P. O. Box 951
Wilmington, DE 19899
(302) 984-6000
provner@potteranderson.com

Attorneys for Plaintiff
ZymoGenetics, Inc.

OF COUNSEL:

Paul J. Andre
Lisa Kobialka
KING & SPALDING LLP
1000 Bridge Parkway
Suite 1000
Redwood City, CA 94065
(650) 590-0700

Dated: May 16, 2008
Public Version: May 22, 2008

I, PAUL J. ANDRE, declare:

1. I am an attorney with the law firm of King & Spalding LLP, counsel of record for Plaintiff ZymoGenetics, Inc. I have personal knowledge of the facts set forth in this declaration and can testify competently to those facts.

2. Attached hereto as Exhibit 1 is a true and correct copy of U.S. Patent No. 5,843,725.

3. Attached hereto as Exhibit 2 is a true and correct copy of U.S. Patent No. 6,018,026, bearing bates numbers ZG000001-77.

4. Attached hereto as Exhibit 3 is a true and correct copy of a ZymoGenetics website printout, available at http://www.zymogenetics.com/about/about.html.

5. Attached hereto as Exhibit 4 is a true and correct copy of the Orencia product insert.

6. Attached hereto as Exhibit 5 is a true and correct copy of pages BMS001290152-62, 1290336, 1290346, 1290366 and 1290843 from the Abatacept BMS-188667 Biologics License Application ("BLA").

7. Attached hereto as Exhibit 6 is a true and correct copy of pages 13-15, 30-31, 52-53 from the transcript of the deposition of Kirk Leister, taken on September 11, 2007.

8. Attached hereto as Exhibit 7 is a true and correct copy of page 6 from the Hood Immunology Textbook.

9. Attached hereto as Exhibit 8 is a true and correct copy of the Expert Rebuttal Report of John Kuriyan, Ph.D. Regarding Non-Infringement of U.S. Patent Nos. 5,843,725 and 6,018,026, dated January 25, 2008.

10. Attached hereto as Exhibit 9 is a true and correct copy of the Expert Report of Jeffrey V. Ravetch, M.D., Ph.D. Regarding Invalidity of U.S. Patent Nos. 5,843,725 and 6,018,026, dated November 20, 2007.

11. Attached hereto as Exhibit 10 is a true and correct copy of the Expert Report of Daniel J. Capon, Ph.D. Regarding Invalidity of U.S. Patent Nos. 5,843,725 and 6,018,026, dated December 3, 2007.

12. Attached hereto as Exhibit 11 is a true and correct copy of pages 25, 27, 30, 56, 63, and 85 from the transcript of Steven Nadler, taken on August 3, 2007.

13. Attached hereto as Exhibit 12 is a true and correct copy of an article authored by Peter Linsley, et al., entitled "Binding Stoichiometry of the Cytotoxic T Lymphocyte-associated Molecule-4 (CTLA-4)," published on June 23, 1995, bearing bates numbers BMS003504385-92.

14. Attached hereto as Exhibit 13 is a true and correct copy of pages 51, 54, 56-57, 60-63, and 82 from the transcript of the deposition of David Smolin, taken on July 18, 2007.

15. Attached hereto as Exhibit 14 is a true and correct copy of pages 262-264 and 272-273 from the transcript of the deposition of David Ostrov, taken on May 6, 2008.

16. Attached hereto as Exhibit 15 is a true and correct copy of an article authored by Johann Deisenhofer, entitled "Crystallographic Refinement and Atomic Models of a Human Fc Fragment and Its Complex with Fragment B of Protein A from *Staphylococcus aureu* at 2.9- and 2.9A Resolution," published on April 28, 1981.

17. Attached hereto as Exhibit 16 is a true and correct copy of an article authored by Paul Carter, et al., entitled "Contribution of Domain Interface Residues to the

Stability of Antibody CH3 Domain Homodimers," published on June 6, 1998, bearing bates numbers ZG054363-54370.

18. Attached hereto as Exhibit 17 is a true and correct copy of Bristol's Objections and Responses to Plaintiff's First Set of Requests for Admission (Nos. 1-83) to Defendant Bristol-Myers Squibb Co., dated October 5, 2007.

19. Attached hereto as Exhibit 18 is a true and correct copy of page 63 to the transcript of the deposition of Steven Nadler, taken on September 20, 2007.

I declare under penalty of perjury under the laws of the State of California and the United States that each of the above statements is true and correct.

Executed on May 16, 2008 in Redwood Shores, California.

Paul J. Andre

EXHIBIT 9

THIS EXHIBIT HAS BEEN REDACTED IN ITS ENTIRETY

EXHIBIT 10

THIS EXHIBIT HAS BEEN REDACTED IN ITS ENTIRETY

EXHIBIT 11

THIS EXHIBIT HAS BEEN REDACTED IN ITS ENTIRETY

EXHIBIT 12

THIS EXHIBIT HAS BEEN REDACTED IN ITS ENTIRETY

EXHIBIT 13

THIS EXHIBIT HAS BEEN REDACTED IN ITS ENTIRETY

EXHIBIT 14

THIS EXHIBIT HAS BEEN REDACTED IN ITS ENTIRETY

EXHIBIT 15

Biochemistry

© Copyright 1981 by the American Chemical Society Volume 20, Number 9 April 28, 1981

Crystallographic Refinement and Atomic Models of a Human Fc Fragment and Its Complex with Fragment B of Protein A from *Staphylococcus aureus* at 2.9- and 2.8-Å Resolution†

PENGAD 800-631-6989 Ostrov DEPOSITION EXHIBIT 16 PTC 5-6-08

Johann Deisenhofer

ABSTRACT: The model of human Fc fragment was refined at 2.9-Å resolution. Two different automated procedures for crystallographic refinement were used [Deisenhofer, J., & Steigemann, W. (1975) *Acta Crystallogr., Sect. B B31*, 238; Jack, A., & Levitt, M. (1978) *Acta Crystallogr., Sect. A A34*, 931]. The final *R* value is 0.22. The dimer of CH3 domains closely resembles the CH1–CL aggregate in Fab fragments. There is no contact between CH2 domains. The contact between CH2 and CH3 domains has about one-third of the size of the CH3–CH3 contact. The carbohydrate, a branched chain of nine hexose units, covers part of the C-contact face of the CH2 domain, shielding hydrophobic residues on this surface. Six atoms of the carbohydrate are within hydrogen-bonding distance of atoms in the CH2 domain. Crystallographic refinement of the complex between Fc fragment and fragment B of protein A from *Staphylococcus aureus* reduced the *R* value of the model to 0.24. A major part of the structure of fragment B consists of two α helices; the rest of the polypeptide chain is folded irregularly. In the crystal, fragment B forms two contacts with Fc fragment molecules. Contact 1 involves residues from both helices of fragment B, and residues from the CH2 and CH3 domains of Fc, and is predominantly hydrophobic. Contact 2 is smaller than contact 1. Residues from the second helix and adjacent residues of fragment B and residues only from the CH3 domain of Fc contribute to contact 2. The nature of contact 2 is mainly polar and includes a sulfate ion. There are strong arguments that contact 1 is the fragment B–Fc contact formed in solution under physiological conditions, while contact 2 is a crystal contact.

The Fc fragment of an immunoglobulin molecule is the dimer of the two C-terminal constant-homology regions of the heavy chain. Among its physiological functions are interactions with the complement system and with specific receptors on the surface of a variety of cells.

The crystal structure of an IgG Fc fragment, obtained from pooled human serum, was studied at 4- (Deisenhofer et al., 1976a) and at 3.5-Å resolution (Deisenhofer et al., 1976b) with the method of multiple isomorphous replacement. These studies revealed the quaternary structure of the molecule and the location of the carbohydrate moiety, which is covalently attached to the CH2 domain. The folding of the polypeptide chain was described on the basis of a preliminary atomic model.

Protein A is a constituent of the cell wall of *Staphylococcus aureus*. Part of its polypeptide chain is a series of four highly homologous regions (Sjodahl, 1977), each of which is able to bind to the Fc part of IgG from various species. Protein A is widely used as a tool in immunochemical and related studies. Its biological role is unknown.

The crystal structure of the complex formed by human Fc fragment and fragment B of protein A was solved by using multiple isomorphous replacement and the known model of the Fc fragment (Deisenhofer et al., 1978). The binding site of FB[1] to Fc fragment and the tertiary structure of FB in the complex was described.

For improvement of both models, the Fc fragment and the FB–Fc complex, and to allow a more detailed description, a crystallographic refinement was done. In this paper I describe the crystallographic refinement and the resulting refined models of the Fc fragment and the FB–Fc complex.

Experimental Methods

Crystal Data. The human Fc fragment crystallizes in space group $P2_12_12_1$ with unit cell dimensions of $a = 80.4$, $b = 146.4$, and $c = 50.4$ Å. There is one Fc fragment molecule in the asymmetric unit (Deisenhofer et al., 1976a). X-ray intensity data were collected by film methods using screenless precession and rotation techniques. For the native data set, 76 films, taken from 23 crystals, were evaluated as described by

† From the Max-Planck-Institut fuer Biochemie, D-8033 Martinsried, West Germany. *Received September 22, 1980.*

[1] Abbreviations used: mir, multiple isomorphous replacement; rms, root mean square; F_{obsd}, observed structure factor; F_{calcd}, calculated structure factor; α_{calcd}, calculated phase angle; *B*, temperature factor; Fab, antigen-binding fragment consisting of light chain and the N-terminal half of the heavy chain; FB, fragment B of protein A; Fc, C-terminal half of the heavy chain with the inter-heavy-chain disulfide bond intact; CH1, CH2, and CH3, the constant homology regions of the heavy chain; hinge peptide, the segment connecting CH1 and CH2 and containing the disulfide linkage between the two heavy chains; C face, the face on a C domain that is involved in the C–C type aggregation.

0006-2960/81/0420-2361$01.25/0 © 1981 American Chemical Society

Schwager et al. (1975). Significant intensities were measured for 48 829 observations of 10 342 independent reflections to 2.9-Å resolution. This is 75% of the total number of reflections in this resolution range; between 3.0- and 2.9-Å resolution, the fraction of significantly measured intensities was 37%. Data from individual films were merged together and scaled by using the method and program of Steigemann (1974). After this procedure, R_{scale} was 0.077

$$R_{scale} = \sum|I(i) - \langle I\rangle|/I(i)$$

[$I(i)$ is the intensity value of an individual measurement, and $\langle I\rangle$ is the corresponding mean value; the summation is over all measurements].

The crystals of the FB–Fc complex belong to space group $P3_121$; the unit cell dimensions are $a = b = 70.6$ Å and $c = 147.4$ Å. The complex lies on a crystallographic diad; thus, the asymmetric unit contains one CH2 domain, one CH3 domain, and one B fragment from protein A. Evaluation of 41 films for 11 crystals yielded 25 876 significant reflection intensities for 7002 unique reflections to 2.8-Å resolution with $R_{scale} = 0.079$. This is 62% of the total number of reflections. The intensities of 3626 independent reflections were below the significance level.

Starting Models. The starting model for crystallographic refinement of the Fc fragment was obtained as described by Deisenhofer et al. (1976b): An electron-density map at 3.5-Å resolution was calculated with phases from multiple isomorphous replacement. By use of an optical comparator, wire models of one CH2 domain and one CH3 domain, both belonging to chain 1, were built on the basis of the amino acid sequence of the human myeloma protein Eu (Rutishauser et al., 1970). Atomic coordinates read from the model were idealized with Diamond's (Diamond, 1966) model building procedure; the fit to the electron density was improved by Diamond's (Diamond, 1971) real-space refinement procedure. The branched carbohydrate chain attached to the CH2 domain was built in three segments by using known hexose geometry. One segment consisted of five hexose units and the other two of two hexose units each; the links between the segments remained uncertain. After generation of coordinates for chain 2 of the Fc fragment by using the known local symmetry and performance of additional rigid-body refinement and real-space refinement, structure factors were calculated with the coordinates of 2788 well-defined atoms from residues Pro-238 to Ser-442 in both chains. An overall temperature factor of 21.3 Å^2 was used as determined from a Wilson plot. The R value for all data between 5- and 2.9-Å resolution was 0.44 ($R = \sum||F_{obsd}| - |F_{calcd}||/\sum|F_{obsd}|$).

The starting model for refinement of the FB–Fc–complex was based on an electron-density map calculated with mir phases at 3.5-Å resolution (Deisenhofer et al., 1978). One CH2 domain and one CH3 domain from a partially refined Fc fragment model (stage 8) were fitted to the density by rigid-body transformation. Electron density was missing for about one-third of the CH2 domain. The protein A fragment model was built with a graphics display system using an electron-density map calculated with combined mir and Fc fragment model phases at 2.8-Å resolution.

Crystallographic Refinement. Two different methods of cyclic crystallographic refinement were used. Part 1 of the refinement began with the method described by Deisenhofer & Steigemann (1975). One refinement cycle included calculation of structure factors from model atomic coordinates, calculation of an electron-density map by using data with Bragg spacings between 7 and 2.9 Å with the coefficients $(n|F_{obsd}| - (n-1)|F_{calcd}|)\exp(i\alpha_{calcd})$, $1 \le n \le 3$, and fitting of the model to this map with Diamond's (Diamond, 1971, 1974) real-space refinement procedure. The resulting coordinates were used as input for the next cycle of refinement. The electron-density maps were calculated with a grid spacing of 0.9 Å. Reflections with $2||F_{obsd}| - |F_{calcd}||/(|F_{obsd}| + |F_{calcd}|) > 1.2$ were omitted from Fourier summation. The real-space refinement procedure works with fixed values for bond lengths, most bond angles, and some torsion angles. A "molten zone" of between 2 and 10 residues slides along the chain; only atoms within the molten zone can move. In the study described here, the length of the molten zone was 6 residues. The φ and ψ torsion angles of the main chain and torsion angles $\chi_1 - \chi_4$ of the side chains were flexible. Flexible $\tau(N–C^\alpha–C)$ bond angles were introduced in an advanced stage of the refinement. Due to the low resolution of the data, real-space refinement produced a number of close interatomic contacts. These bad contacts were removed with an energy-refinement program (Levitt & Lifson, 1969; Levitt, 1974).

In part 2 of the refinement, the method of Jack & Levitt (1978) was used instead of real-space refinement. This method derives the normal equations for a diagonal-matrix least-squares refinement from a difference-Fourier map. The crystallographic residual $\sum(|F_{obsd}| - |F_{calcd}|)^2$ is then minimized together with the conformational energy of the model. The relative weights of crystallographic residual and conformational energy can be set through a scale factor. The value of this scale factor decides whether idealized model geometry is strictly kept or relaxed in favor of a smaller crystallographic residual. Energy parameters for bond lengths, bond angles, torsion angles, and nonbonded interactions were those recommended by Levitt (1974), except that proline rings were kept flat with torsion-angel potentials similar to the ones used for aromatic rings. Difference-Fourier maps were calculated with grid spacings of one-third of the resolution limit. The resolution range varied between 7–4 Å and 7–2.9 Å.

The diagonal-matrix least-squares method was also used to refine isotropic temperature factors. Individual B values of the atoms of each residue were averaged to give one B value per residue.

Typically, the automated refinement reached a local minimum of crystallographic R value after about four cycles of either procedure, at which point the errors remaining in the model required shifts of atomic coordinates greater than the radius of convergence of the refinement method in use. In order to detect such errors and to get an idea of the necessary corrections, I carried out the following steps: In part 1 of the refinement, difference-Fourier maps were calculated and plotted on paper along with the model atomic coordinates. Corrections to the model deduced from the map were applied either with an option of the real-space refinement program, which allows input of desired values for torsion angles or atomic positions which the program then tries to realize, or with Diamond's model-building program.

In part 2 of refinement, inspection of maps and modifications of the model were significantly simplified by the use of an interactive graphics display system. The most helpful features of this system, programmed by Jones (1978), are rotation around bonds, shifting of atoms or atom groups, and changes of the chemical sequence. If necessary, ideal geometry can be restored after such operations with a modified version of the model-building program of Hermans & McQueen (1974). Maps calculated with coefficients $2|F_{obsd}| - |F_{calcd}|$ and either model phases, Sim-weighted model phases (Hendrickson & Lattman, 1970), or phases resulting from combination of model phases and mir phases (Hendrickson & Lattman, 1970)

were used with the display. In the phase combination procedure, model phases and mir phases were given equal weights. Structure factors, R values, and electron-density maps were calculated with Steigemann's "PROTEIN" program system (Steigemann, 1974). The refinement of the FB–Fc complex was done in parallel with Fc fragment refinement by using identical methods.

Accessible Surface Areas and Hydrogen Bonds. The various interdomain contacts in Fc fragment and FB–Fc complex were investigated by calculating and comparing the accessible surface areas of separate domains and composite molecules. A computer program, based on the method of Lee & Richards (1971) and written by Levitt (personal communication; Chothia, 1975), was used for these calculations. The probe size, i.e., the radius of a water molecule, was set to 1.4 Å. The method assumes the molecules to be rigid. Atoms which are mobile in the crystal were included in the calculations.

A second option of Levitt's program was used to search for hydrogen bonds. The proposed hydrogen bond candidates with a donor–acceptor distance of <3.5 Å were checked by eye at the display system to see whether they approximately met the geometric requirements for hydrogen-bond formation.

Amino Acid Sequence Homologies. For comparison of amino acid sequences of different domains and antibody molecules, the table composed by Beale & Feinstein (1976) was used.

Results and Discussion

Crystallographic Refinement of Fc Fragment. The course of Fc fragment refinement part 1 (Diamond refinement) and part 2 (Jack–Levitt refinement) is listed in Tables Ia and Ib (see paragraph at end of paper regarding supplementary material). On the average, four cycles of automated refinement were carried out between calculation of the maps.

Between the start of refinement and step 3, the second difference-Fourier map, the R value was reduced by 0.06. Between steps 3 and 7, R decreased very slowly. The introduction of free τ(N–C$^\alpha$–C) angles resulted in a larger decrease of R between steps 7 and 8. After step 8, the Jack–Levitt refinement was begun with an initial scale factor between crystallographic residual and conformational energy of 10^{-4}; this scale factor was later decreased to 3×10^{-5}. The large decrease of R between steps 8 and 9 [Table Ib (supplementary material)] was at least in part due to relaxation of geometric constraints, which led to a high energy of the model. Between steps 9 and 11, mainly the energy was lowered at constant R. In the final steps 11–15, further corrections of the model reduced both R and the conformational energy. In steps 9–15, whenever large manual changes of the model were done, subsequent automated refinement was started at 7–4-Å resolution to increase the radius of convergence (Jack & Levitt, 1978). In the following cycles, the upper resolution limit was gradually increased to 2.9 Å. The refinement converged at an R-value of 0.22 for reflections between 7- and 2.9-Å resolution.

Average residue temperature factors were updated before inspection of each new map. When individual B values were averaged, the minimum allowed value was set to 6 Å^2.

Due to the low resolution, the difference-Fourier maps were difficult to interpret. In many cases, incorrect parts of the model could be recognized clearly from negative density; the corresponding positive density which indicates the correct atomic positions was often rather weak and difficult to interpret. The situation was not improved when atoms with uncertain positions were left out of the structure factor calculation. The interpretation of the $2|F_{obsd}| - |F_{calcd}|$ maps was found less difficult. Electron density for many of the atoms with uncertain positions, which were left out from the structure factor calculation, could be found. In cases where the model did not coincide with the electron density, it was possible to try different model conformations in search of a better fit. The $2|F_{obsd}| - |F_{calcd}|$ maps calculated with combined model and mir phases provided the clearest guide to necessary changes in the model. Phase combination also allowed inclusion of low-resolution reflections (those with Bragg spacings >7 Å) in the Fourier summation. As with most refined protein structures, the fit between observed and calculated structure factors at low resolution is very poor; for this reason, model phases of reflections inside the 7-Å sphere were not used except in combination with mir phases.

In general, corrections to the model made "by hand" were influenced by the inspected map, by stereochemical considerations (plausible conformation, contacts to neighbors), and by comparison of the two crystallographically independent polypeptide chains of the Fc fragment molecule. On several occasions, polypeptide segments of up to five residues were deliberately built with different conformation in both chains to see which one would fit better to the electron density after the next cycles of automated refinement. The mir map was used throughout the refinement of the Fc fragment as an additional guide when the model was changed. After each round of manual corrections to the model, the R value rose by 0.01–0.03; the first one or two cycles of automated refinement were needed to bring R back to the previous level.

Observed structure factor amplitudes of 9332 reflections between 7- and 2.9-Å resolution were used for refinement. During real-space refinement, 2092 conformational angles were flexible parameters. The number of free parameters in Jack–Levitt refinement is more difficult to count, because the relative weight of crystallographic and energy contributions depends on the choice of the scale factor. A total of 10 596 coordinates of 3532 atoms (of which only 3182 contributed to calculated structure factors during the final cycles) were restrained by 3646 bond lengths, 4998 bond angles, and 6072 torsion angle potentials. A total of 1598 torsion angles had energy barriers of 20 kcal/mol or more. About 40 000 atom pairs with distances less than the sum of the van der Waals radii plus 2.0 Å contributed to the nonbonded interaction energy; pairs of atoms which occur in a bond, a bond angle, or a torsion angle were excluded from the list of nonbonded interactions.

During this work, the following main advantages of the Jack–Levitt refinement method were noticed: (a) refinement at low resolution is possible, (b) geometric restraints can be relaxed temporarily, (c) treatment of branched chains is easy, (d) the method requires ~30% less computing time than Diamond's real-space refinement, (e) distorted geometry can be repaired, and (f) refinement of temperature factors at 2.9-Å resolution is possible.

The rms difference between C$^\alpha$ coordinates of chain 1 of the starting and refined models is 1.18 Å for 158 of the 206 residues. This value is very large compared to the rms C$^\alpha$ shift of 0.45 Å during refinement of the pancreatic trypsin inhibitor (Deisenhofer & Steigemann, 1975), where the initial model was based on a mir map at 1.9-Å resolution.

In each polypeptide chain 38 residues and the carbohydrate moiety had to be rebuilt during refinement. These residues belong to segments Val-284 to His-310, Pro-353 to Met-358, Asn-384 to Asn-390, Gly-402, Glu-430 to His-435, and Leu-443, which was not present in the starting model. For residues 385–389, the amino acid sequence was changed from

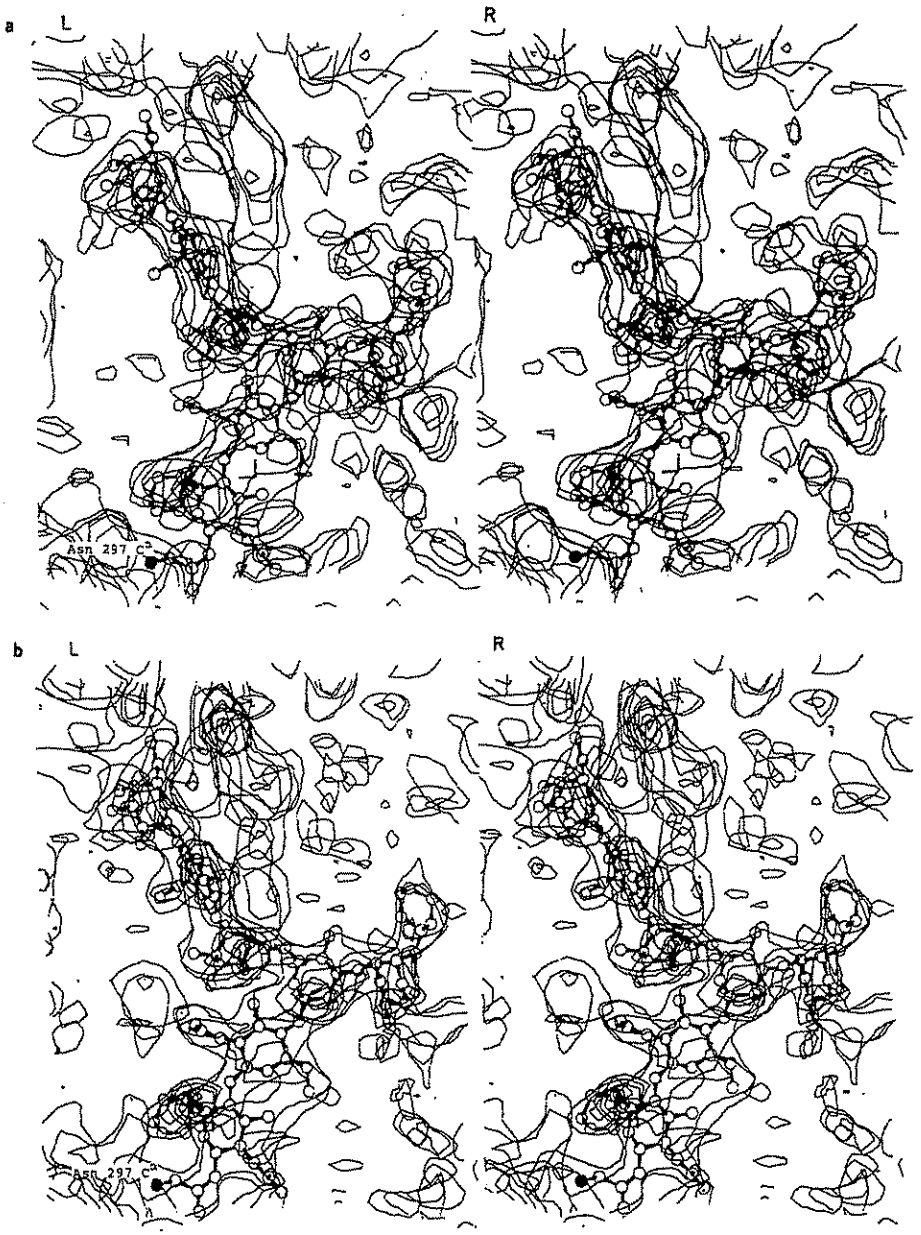

FIGURE 1: Stereo drawings of refined model of carbohydrate and side chain of Asn-297 (only atoms contributing to F_{calcd}): (a) the mir map (3.5-Å resolution; contour levels at 0.17 and 0.51 e/Å^3) and (b) the final $2|F_{obsd}| - |F_{calcd}|$ map (2.9-Å resolution; combined mir and model phases; contour levels at 0.25 and 0.75 e/Å^3). Parts of the electron density belong to the protein; the corresponding model was omitted.

Asp-Gly-Glu-Pro-Glu to Gly-Gln-Pro-Glu-Asn (Ponstingl & Hilschmann, 1972; Hofmann & Parr, 1979). Only the later amino acid sequence is compatible with the electron density. No interpretable electron density could be found for residues Thr-223 to Gly-237, which include almost the whole hinge region with the inter-heavy-chain disulfide bridges. At the C-terminal end, residues 444–446 remained undefined. The carbohydrate model includes 9 of the 12 possible hexose units (Kornfeld & Kornfeld, 1976). Figure 1 shows for comparison the refined carbohydrate model (chain 1) drawn into both the mir map and the final $2|F_{obsd}| - |F_{calcd}|$ map calculated with combined phases.

The average temperature factor in both CH3 domains is 19.5 Å^2; in contrast, CH2 of chain 1 has an average B of 25 Å^2, and for CH2 of chain 2, the average B is 30 Å^2. These values demonstrate that in crystals of Fc fragment, the CH2 domains are less well ordered than the CH3 domains; CH2 of chain 2 is more disordered than CH2 of chain 1.

Bond lengths and bond angles of the refined model are very close to ideal values; the rms deviations are 0.007 Å and 1.7°, respectively. The rms deviation of ω and similar angles from minimum energy values if 5.9°. For the torsion angles which keep aromatic rings planar, the rms deviation is 1.8°.

An estimate of the accuracy of the refined Fc fragment coordinates can be obtained from comparison of chain 1 and chain 2. A total of 340 main-chain atoms from 85 residues of CH3 chain 1 with temperature factors below 35 Å^2 were rotated onto the corresponding atoms of chain 2. After least-squares refinement of the transformation parameters, the rms distance of equivalent atom positions was 0.29 Å. This

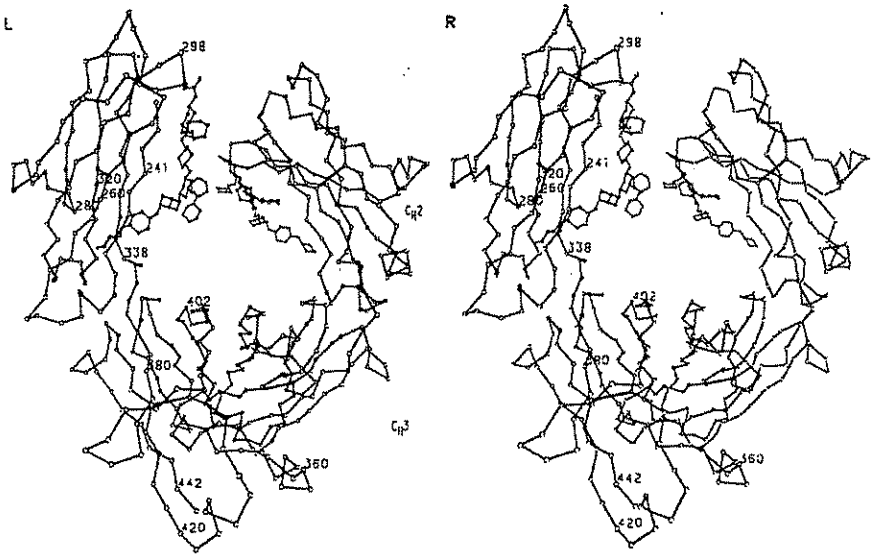

FIGURE 2: Stereo drawing of Fc fragment model (C^α) with carbohydrate (hexose rings, glycoside linkages, and Asn-297 side chain). Selected residues of chain 1 are labeled with residue numbers (residue numbering from myeloma protein Eu). Disulfide bridges are indicated by thick lines.

number is a rough estimate of the accuracy of coordinates which could be achieved in regions of high crystalline order. In regions with less order, the coordinate errors can be considerably larger. Such regions exist mainly in the CH2 domains. At 2.9-Å resolution carbonyl oxygens of the main chain cannot be located unambiguously in the electron-density map to determine the peptide orientations. This problem is less serious in regions with secondary structure. Outside these regions, especially in zones with high temperature factors, peptide orientations may be wrong even in the refined model.[2]

Crystallographic Refinement of FB–Fc Complex. The course of refinement of the FB–Fc complex model was very similar to that of Fc fragment and is briefly summarized here: The R value of the starting model was 0.40. Six cycles of real-space refinement using $2|F_{obsd}| - |F_{calcd}|$ maps calculated with model phases reduced the R value to 0.34. After additional cycles of Jack–Levitt refinement, the final R value was 0.24 for 6243 reflections between 7- and 2.8-Å resolution.[2] Energies and deviations of model parameters from ideal values are close to the values obtained for Fc fragment. Errors detected and corrected in the model of Fc fragment were corrected simultaneously in the Fc part of FB–Fc. To check these modifications and the model of the FB part, I inspected several $2|F_{obsd}| - |F_{calcd}|$ maps calculated with combined mir and model phases. Refinement of large parts of the CH2 domain and of parts of FB was hampered by poor crystalline order.

Description of Fc Fragment Model. Figure 2 shows a C^α drawing of Fc fragment, together with the attached carbohydrate chain. CH2 domains and CH3 domains are folded into two layers of antiparallel β-sheet structure which enclose a predominantly hydrophobic interior, a design typical for all immunoglobulin domains. The aggregation of CH3 domains is similar to that of the CH1–CL dimers in Fab fragments (Poljak et al., 1974; Segal et al., 1974; Matsushima et al., 1978; Marquart et al., 1980). The CH2 domains do not form a lateral contact with each other. Part of the CH2 C-contact face is covered by carbohydrate. The carbohydrate forms a weak bridge between CH2 domains.

Within the limits of error, the local symmetry axis relating CH3 domains is a diad. Expressed in polar angles, the rotational part of the transformation from CH3 chain 1 to CH3 chain 2 is $\varphi = 6.5$, $\psi = -100$, and $\kappa = -179.3$ (φ is the angle between the rotation axis and the y axis; ψ is the angle between the x axis and the projection of the rotation axis into the x–z plane; κ is the rotation angle). The loal symmetry axis relating CH2 domains with polar angles of $\varphi = 8.6$, $\psi = -100$, and $\kappa = -174.3$ differs from the CH3–CH3 axis by 2° in direction; the rotation angle differs by ~5° from a 2-fold rotation. In addition, the CH2–CH2 rotation is accompanied by a screw component of 1.1 Å. The differences between the local symmetries of CH2 and CH3 reflect flexibility in the CH2–CH3 contact region.

Table II (supplementary material) is a list of the possible hydrogen bonds between Fc fragment and carbohydrate. The table does not contain main-chain hydrogen bonds; these are shown in Figures 3 and 5.

CH2 Domain and Carbohydrate. Since the crystalline order is considerably better in CH2 chain 1 than in chain 2, the following description is based exclusively on the chain 1 model. The domain folding scheme with main-chain hydrogen bonds is shown in Figure 3. From the hydrogen bonding pattern, the layers of antiparallel β sheet can be clearly distinguished. Layer 1, which is equivalent to the C-contact face in CL, CH1, and CH3 domains, consists of four strands: Ser-239 to Phe-243, Thr-256 to Val-264, Lys-290 to Tyr-296, and Thr-299 to Leu-309. Layer 2 has three long strands: Lys-274 to Val-279, Glu-318 to Asn-325, and Ile-332 to Ile-336; residues Val-282 to Val-284 form a short piece of a fourth strand.

The carbohydrate moiety is attached to Asn-297 at the bend between strands 3 and 4 of layer 1. Figure 4 shows, in a series of three stereo drawings, the refined carbohydrate model and its position with respect to the CH2 domain; Figure 4c also shows the CH2 side chains involved in the contact. The CH2–carbohydrate contact is described in terms of the decrease of accessible surface area in Table III (supplementary material). The majority of buried CH2 residues are in strands

[2] Refined atomic coordinates of the Fc fragment and of the FB–Fc complex are available upon request. The coordinate sets also have been sent to the Protein Data Bank of Brookhaven National Laboratory, Upton, NY.

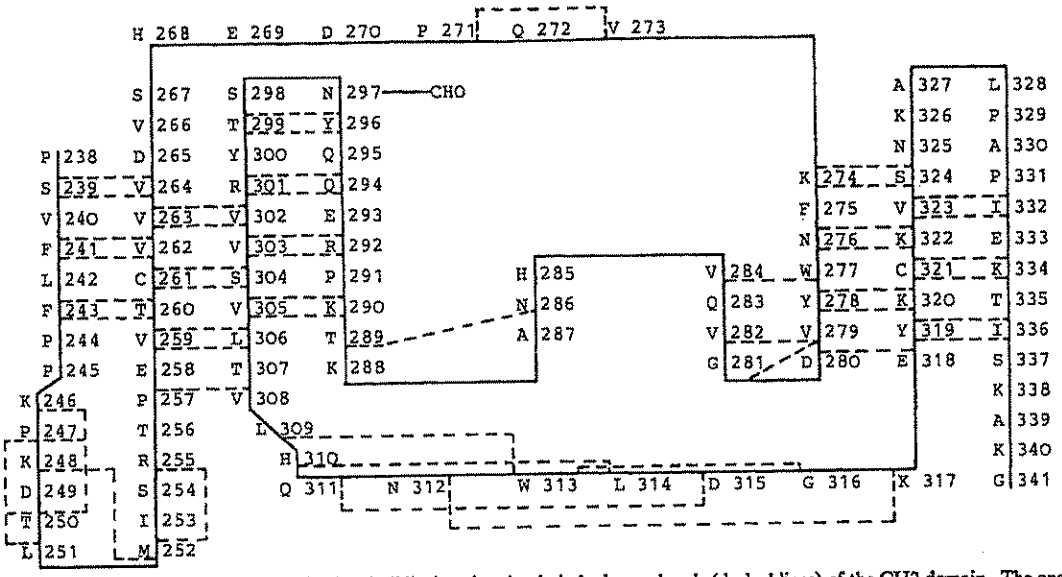

FIGURE 3: Schematic representation of chain folding (full line) and main-chain hydrogen bonds (dashed lines) of the CH2 domain. The one-letter code for amino acids is used.

1 and 2 of the C-contact face. Both hydrophobic and polar residues are involved. Six CH2 side chain atoms are within hydrogen-bonding distance to polar atoms of the carbohydrate; within the carbohydrate itself, six single additional hydrogen bonds are possible [Table II (supplementary material)]. Five of these are between adjacent hexose units: three between O3 and O5, one between O3 and O6, and one between O3 and O2. H bonds of this kind have been found in crystal structures of small polysaccharides [for a review, see Sundararajan & Marchessault (1979)]. With the exception of Asp-265, Asn-297, and Thr-299, the CH3 residues in structural positions analogous to the ones listed in Table III (supplementary material) are involved in the CH3–CH3 contact. This demonstrates that the carbohydrate in CH2 provides a substitute for the C–C contact and presumably helps to stabilize the CH2 domain. However, upon formation of the CH3–CH3 contact, about twice as much surface area [1090 Å^2; Table IV (supplementary material)] is covered per domain as in the CH2–carbohydrate contact (522 Å^2). This observation could explain the apparent "softness" of those parts of the CH2 domain which are most remote from the CH2–CH3 interface, which is indicated by large temperature factors or missing electron density. The difference of the temperature factors of CH2 chain 1 and chain 2 appears to be the result of different crystal environments: CH2 chain 1 is in contact with neighboring CH2 domains in the crystal at residues His-268, Lys-274, His-285, and Asn-297. In chain 2 these crystal contacts are missing; as a consequence, residues Val-266 to Asp-270, Gln-295 to Arg-301, and three hexose units (two *N*-acetylglucosamines and fucose) are disordered. The disorder in CH2 is even more pronounced in crystals of the FB–Fc complex, where the CH2 domain also lacks crystal contacts. Partial disorder of the CH2 domain can therefore be expected in solution. However, in the presence of the Fab arms, the CH2 domain might become ordered if a suitable Fab–CH2 contact is formed in an intact IgG molecule.

CH3 Domain and Contacts CH3–CH3 and CH2–CH3. Figure 5 shows a schematic drawing of the CH3 polypeptide chain with main-chain hydrogen bonds. Four strands of antiparallel β sheet are part of the C-contact face: residues Gln-342 to Leu-351, Glu-362 to Tyr-373, Asn-390 to Leu-398, and Ser-403 to Asp-413. The β-sheet geometry is severely distorted at residues Pro-343, Pro-346, Gly-371, Pro-395, and Pro-396. In the second face of the molecule, β strands are formed by residues Ile-377 to Glu-382, Val-422 to His-429, and Tyr-436 to Leu-443. As in CH2, a fourth strand is formed by residues Gln-386 to Glu-388. Residue Pro-374 is a *cis*-proline; the homologous proline residues in CH1 and CL of Fab Kol (Marquart et al., 1980) and in CH1 of Fab New (Saul et al., 1978) were also reported to be in cis conformation.

The loss of accessible surface area of individual residues upon formation of the CH3–CH3 contact is listed in Table IV (supplementary material). A total of 2180 Å^2 of accessible surface area is covered in the CH3 module. Possible inter-CH3 hydrogen bonds or charge interactions are shown in Table II (supplementary material). Almost all the residues involved in the CH3–CH3 contact are in positions homologous to the ones which participate in the CH1–CL contact in Fab Kol (Marquart, 1980) and in Fab New (Saul et al., 1978). Exceptions are Gln-347, Asn-390, and Thr-393. The interdomain salt bridge between Glu-357 and Lys-370 [Table II (supplementary material)] has its homologous equivalent in both Fab Kol and Fab New.

The residues involved in the CH2–CH3 contact are listed in Table V (supplementary material). With an accessible surface area of 778 Å^2 covered, this contact has roughly one-third of the size of the CH3–CH3 contact. According to Beale & Feinstein (1976), Leu-251, the most important hydrophobic residue in the contact, is conserved in IgG of man, mouse, guinea pig, and rabbit, in human IgA, and in the CH3 domain of human IgE. In CH3 of human IgM, the homologous residue is Ile. Other highly conserved contact residues are Pro-247, Met-252, Lys-338, Pro-374, Asp-376, Ile-377, and Glu-430.

Polar interactions in the CH2–CH3 contact are listed in Table II (supplementary material). The salt bridge between Lys-338 and Glu-430 appears to be a characteristic component of this type of contact. Lys-338 is conserved in CH2 domains

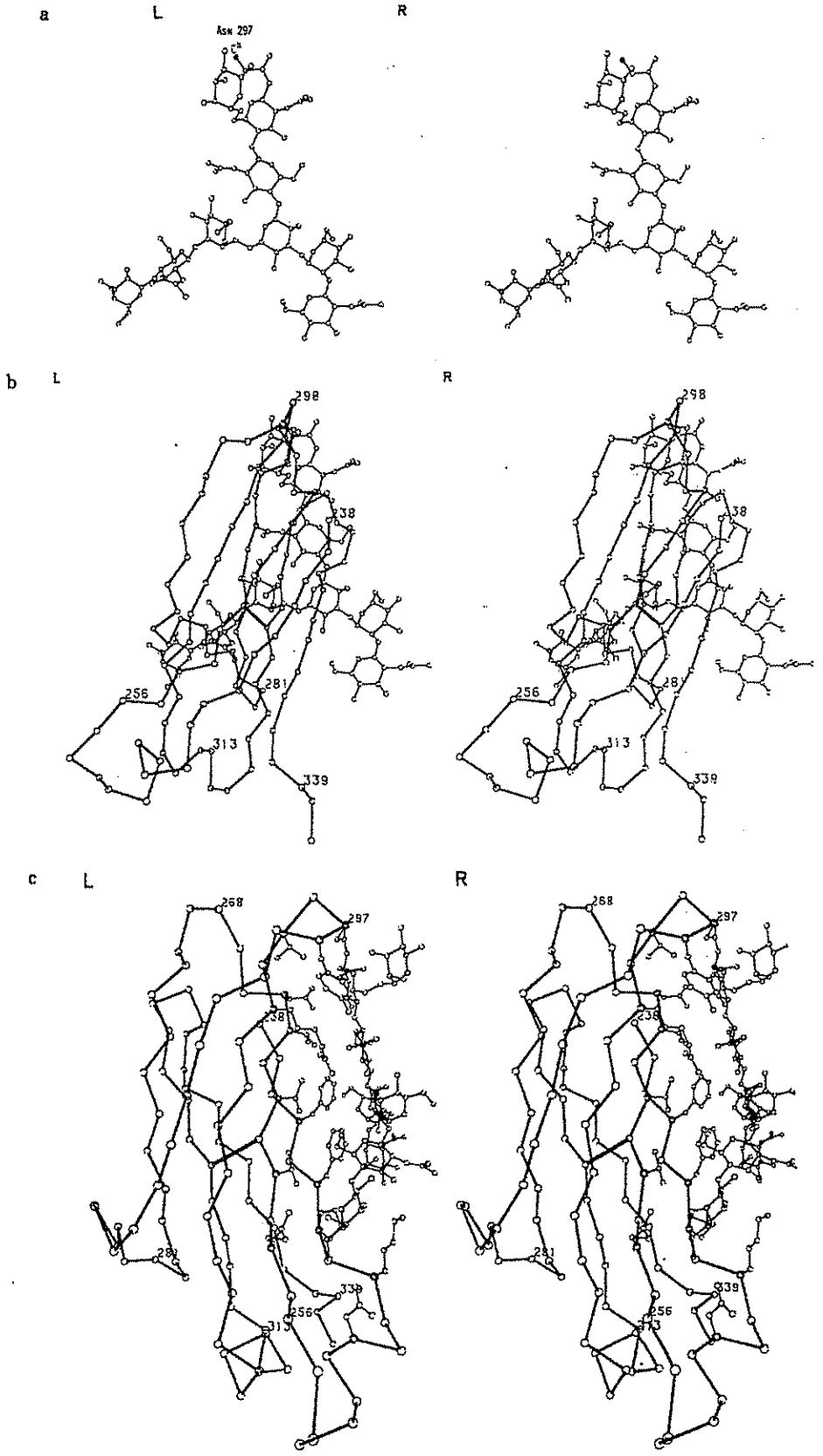

FIGURE 4: Stereo drawings of the carbohydrate and its interaction with the CH2 domain: (a) carbohydrate and side chain of Asn-297; (b) carbohydrate and C^{α} model of CH2 domain; (c) carbohydrate and C^{α} model of CH2 and CH2 side chains involved in the contact.

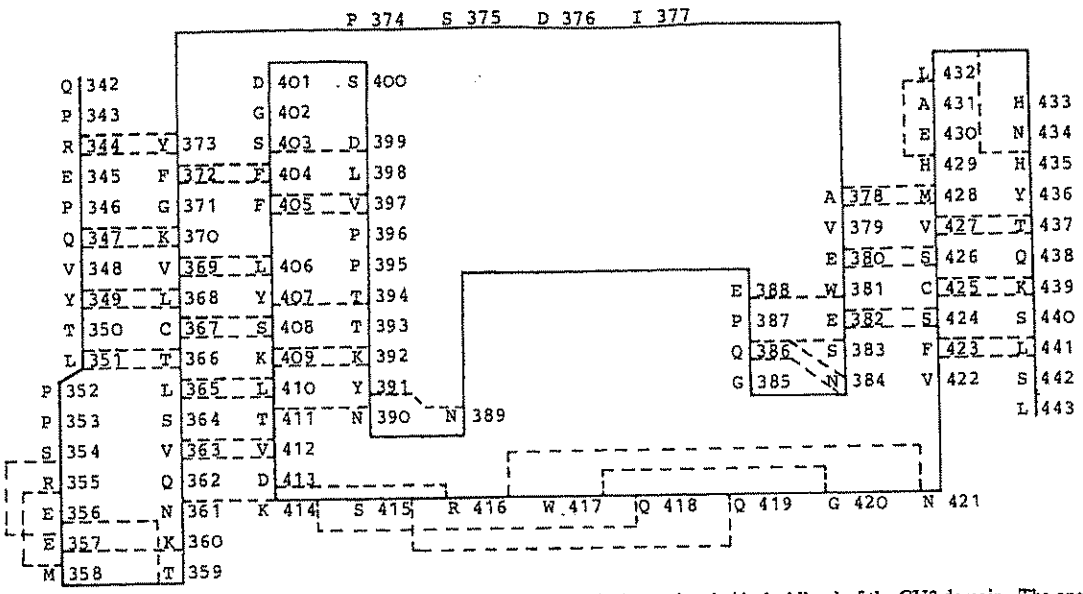

FIGURE 5: Schematic representation of chain folding (full line) and main-chain hydrogen bonds (dashed lines) of the CH3 domain. The one-letter code for amino acids is used.

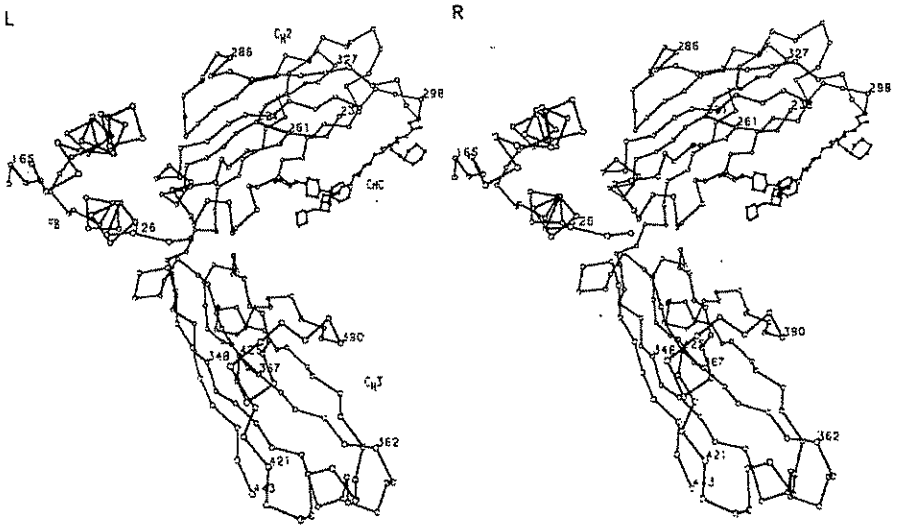

FIGURE 6: Stereo drawing of a monomer of the FB–Fc complex. Disordered regions in CH2 and in carbohydrate are indicated by reduced thickness of lines.

of IgG from man, mouse, guinea pig, and rabbit and in CH3 of human IgE; CH3 of human IgM has Arg instead of Lys. In human IgA, the homologous residue is Ser, but with Lys next to it. Glu-430 is conserved in CH3 of IgG and IgA and in CH4 of IgM and IgE; an exception is mouse IgG1 (MOPC 21), in which Gln was reported at this position. These sequence homologies indicate that the CH2–CH3 contact described here is very likely to be found in IgG and IgA and as a CH3–CH4 contact also in IgE and IgM.

FB–Fc Complex. Electron density for the FB part of the FB–Fc complex can be found from residues Phe-124 to Glu-166; residues Ala-120 to Lys-123 and Ala-167 to Lys-177 are disordered. Two antiparallel α helices formed by residues Gln-128 to Leu-136 and Glu-144 to Asp-155 are the predominant elements of secondary structure of FB. Table VI (supplementary material) shows the possible hydrogen bonds and charge interactions made by FB in the crystal. A large number of main-chain hydrogen bonds are typical for α helices. For residues Ser-158 to Glu-166, the electron density is weak and allows only the tracing of the polypeptide chain without giving information on peptide orientations.

FB makes two types of contact to symmetry-related Fc fragment chains in the crystal. Upon formation of contact 1, 1234 Å^2 of accessible surface area on FB and Fc is covered. As listed in Table VII (supplementary material), residues from CH2 and CH3 of Fc fragment and from the helical regions of FB are involved. Contact 1 is predominantly hydrophobic; only four hydrogen bonds between FB and Fc contribute to the stability of this contact [Table VI (supplementary material)].

The residues participating in contact 2 are shown in Table VIII (supplementary material). With 1012 Å^2 of accessible surface area covered, this contact is smaller than contact 1. Residues of the second helix and Asp-156 to Gln-159 of FB are covered. From the Fc fragment, only residues of the CH3 domain contribute to contact 2. In addition, a large peak of electron density near contact 2 was interpreted as a sulfate ion from the ammonium sulfate in the crystallization solution.

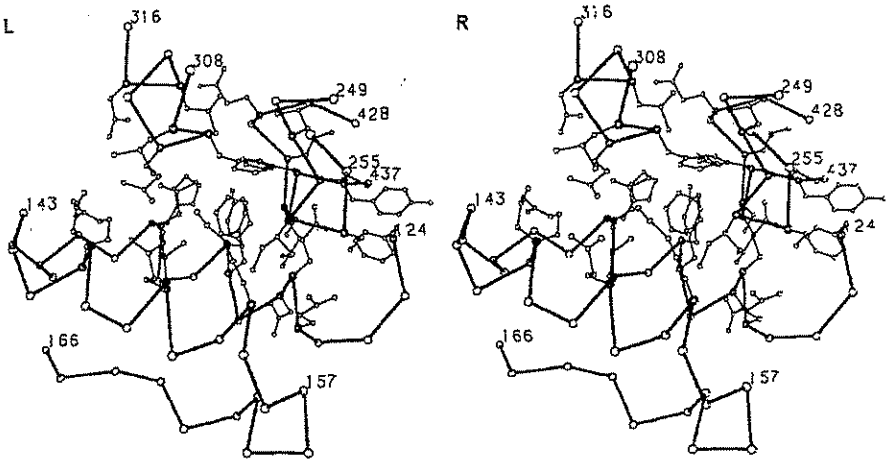

FIGURE 7: Stereo drawing of FB–Fc contact region with amino acid side chains. The course of the main chain of FB and of parts of Fc is drawn in thick lines.

Its negative charges are compensated by Lys-154 of FB and by Arg-416 of Fc. Including the sulfate ion, 14 hydrogen bonds or charge interactions [Table VI (supplementary material)] are observed in contact 2. Among these, the close proximity of Asp-155 of FB and Glu-388 of Fc, which are directly in the center of contact 2, is striking. FB–Bc crystals were grown at pH 4.1 (Deisenhofer et al., 1978); such a low pH appears to be necessary to allow Asp-155 and Glu-388 to be neighbors and the formation of contact 2. This observation and the contribution of a sulfate ion are strong arguments for the assumption that contact 2, although quite intimate, is a crystal contact. In solution, contact 2 should be possible only under conditions similar to the ones in the crystal.

Thus, under physiological conditions, it is most likely that only contact 1 can be formed in solution. Figure 6 shows a monomer of the FB–Fc complex with the molecules forming contact 1. The other half of the molecule is related to the one shown by an exact crystallographic diad. With the exception of small changes due to contact 2 at residues 384, 385, 388, and 416, the CH3 domain of FB–Fc is identical with CH3 in Fc fragment crystals. The CH2 domain of FB–Fc is even more disordered than the CH2 chain 2 of Fc fragment; residues Val-266 to Lys-274, Gln-295 to Tyr-300, and Asn-325 to Pro-331 and four hexose units of the carbohydrate are too mobile to be observed in the electron density. Since binding of protein A does not inhibit complement activation (Wright et al., 1977) and the binding site of C1q to Fc was reported to be on CH2 (Yasmeen et al., 1976), the C1q–Fc interaction must occur somewhere in the more mobile parts of CH2.

Figure 7 is a detailed picture of contact 1 between FB and Fc, including side chains. Ile-253 of Fc is totally covered by residues from FB. Other residues with a shielded area of more than 20 Å^2 are Met-252, Ser-254, Leu-309, His-310, Gln-311, Asn-434, His-435, and Tyr-436 of Fc and Phe-124, Gln-128, Gln-129, Asn-130, Phe-132, Tyr-133, Leu-136, Asn-147, Ile-150, Gln-151, and Lys-154 of FB [Table VII (supplementary material)].

As suggested previously (Deisenhofer et al., 1978), the inability of human IgG3 to form a complex with protein A (Michaelsen et al., 1977; Wolfenstein-Todel et al., 1976) can be explained by the substitution of Arg for His-435 in the Fc fragment. Model building with the display system showed that it is virtually impossible to find a place for the arginine in the complex. Close contacts would occur between the arginine side chain and residues Phe-132 and Leu-136 of FB and Leu-314 of Fc; in addition, the positive charge of the arginine would remain unbalanced. None of the other amino acid exchanges in CH3 of IgG3 (Michaelsen et al., 1977) are near contacts 1 or 2.

Acknowledgments

Discussions with Professor Robert Huber were helpful and stimulating throughout this work. Dr. T. A. Jones helped me to operate the interactive display system. Dr. W. S. Bennett made valuable suggestions which helped to improve the paper. The technical assistance of K. Epp during preparation of the drawings is acknowledged. I thank Drs. Robert Diamond, Michael Levitt, and the late Tony Jack for making their compter programs available to me.

Supplementary Material Available

Tables Ia and Ib (course of crystallographic refinement of Fc fragment), Table II (polar interactions in Fc fragment), Table III (CH2–carbohydrate contact), Table IV (CH3–CH3 contact), Table V (CH2–CH3 contact), Table VI (polar interactions of FB), Table VII (FB–Fc contact 1), and Table VIII (FB–Fc contact 2) (10 pages). Ordering information is given on any current masthead page.

References

Beale, D., & Feinstein, A. (1976) *Q. Rev. Biophys. 9*, 135.
Chothia, C. (1975) *Nature (London) 254*, 304.
Deisenhofer, J., & Steigemann, W. (1975) *Acta Crystallogr., Sect. B B31*, 238.
Deisenhofer, J., Colman, P. M., Huber, R., Haupt, H., & Schwick, G. (1976a) *Hoppe-Seyler's Z. Physiol. Chem. 357*, 435.
Deisenhofer, J., Colman, P. M., Epp, O., & Huber, R. (1976b) *Hoppe-Seyler's Z. Physiol. Chem. 357*, 1421.
Deisenhofer, J., Jones, T. A., Huber, R., Sjodahl, J., & Sjoquist, J. (1978) *Hoppe-Seyler's Z. Physiol. Chem. 359*, 975.
Diamond, R. (1966) *Acta Crystallogr., Sect. A A21*, 253.
Diamond, R. (1971) *Acta Crystallogr., Sect. A A27*, 436.
Diamond, R. (1974) *J. Mol. Biol. 82*, 371.
Hendrickson, W. A., & Lattman, E. E. (1970) *Acta Crystallogr., Sect. B B26*, 136.
Hermans, J., & McQueen, J. E. (1974) *Acta Crystallogr., Sect. A A30*, 730.
Hofmann, T., & Parr, D. M. (1979) *Mol. Immunol. 16*, 923.
Jack, A., & Levitt, M. (1978) *Acta Crystallogr., Sect. A A34*, 931.
Jones, T. A. (1978) *J. Appl. Crystallogr. 11*, 268.

Kornfeld, R., & Kornfeld, S. (1976) *Annu. Rev. Biochem. 45*, 217.
Lee, B., & Richards, F. M. (1971) *J. Mol. Biol. 55*, 379.
Levitt, M. (1974) *J. Mol. Biol. 82*, 393.
Levitt, M., & Lifson, S. (1969) *J. Mol. Biol. 46*, 269.
Marquart, M. (1980) Ph.D. Thesis, Technical University of Muenchen.
Marquart, M., Deisenhofer, J., Huber, R., & Palm, W. (1980) *J. Mol. Biol. 141*, 369.
Matsushima, M., Marquart, M., Jones, T. A., Colman, P. M., Bartels, K., Huber, R., & Palm, W. (1978) *J. Mol. Biol. 121*, 441.
Michaelsen, T. E., Frangione, B., & Franklin, E. C. (1977) *J. Immunol. 119*, 558.
Poljak, R. J., Amzel, L. M., Chen, B. L., Phizacherley, R. P., & Saul, F. (1974) *Proc. Natl. Acad. Sci. U.S.A. 71*, 3440.
Ponstingl, H., & Hilschmann, N. (1972) *Hoppe-Seyler's Z. Physiol. Chem. 353*, 1369.
Rutishauser, U., Cunningham, B. A., Bennet, C., Konigsberg, W. H., & Edelman, G. M. (1970) *Biochemistry 9*, 3171.
Saul, F. A., Amzel, L. M., & Poljak, R. J. (1978) *J. Biol. Chem. 253*, 585.
Schwager, P., Bartels, K., & Jones, T. A. (1975) *J. Appl. Crystallogr. 8*, 275.
Segal, D. M., Padlan, E. A., Cohen, G. H., Rudikoff, S., Potter, M., & Davies, D. R. (1974) *Proc. Natl. Acad. Sci. U.S.A. 71*, 4298.
Sjodahl, J. (1977) *Eur. J. Biochem. 78*, 471.
Steigemann, W. (1974) Ph.D. Thesis, Technical University of Muenchen.
Sundararajan, P. R., & Marchessault, R. H. (1979) *Adv. Carbohydr. Chem. Biochem. 36*, 315.
Wolfenstein-Todel, C., Frangione, B., Prelli, F., & Franklin, E. C. (1976) *Biochem. Biophys. Res. Commun. 71*, 907.
Wright, C., Willan, K. J., Sjodahl, J., Burton, D. R., & Dwek, R. A. (1977) *Biochem. J. 167*, 661.
Yasmeen, D., Ellerson, J. R., Dorrington, K. J., & Painter, R. H. (1976) *J. Immunol. 116*, 518.

Immunological Comparison of Rat, Rabbit, and Human Microsomal Cytochromes P-450†

F. Peter Guengerich,* Philip Wang, Patricia S. Mason, and Margaret B. Mitchell

ABSTRACT: Antibodies were raised in rabbits to electrophoretically homogeneous cytochromes P-450 isolated from rat and human liver microsomes. These antibodies were used to compare various forms of rat, rabbit, and human cytochromes P-450 present in microsomes and in purified preparations by using double-diffusion analysis, immunoelectrophoresis, quantitative microcomplement fixation, competitive radioimmune assay, and inhibition of enzyme activity toward *d*-benzphetamine and benzo[*a*]pyrene. The results indicate that (1) at least some forms of cytochrome P-450 from the three species share certain common immunological determinants, (2) there are immunological differences between cytochromes P-450 isolated from the three species, (3) some immunological differences exist between cytochromes P-450 isolated from rats of different strains, (4) immunologically distinguishable forms of cytochrome P-450 exist within individual human liver samples, and (5) human liver samples obtained from different individuals contain immunologically different forms of cytochrome P-450. Quantitative microcomplement fixation techniques were used to assign immunological distances to different forms of rat, rabbit, and human liver microsomal cytochrome P-450. Cross-reactivity was observed in all systems tested, and the extent of immunological similarity was dependent upon the particular assay used.

Cytochrome P-450[1] serves a pivotal role as the terminal oxidase in a microsomal mixed-function oxidase system that catalyzes the metabolism of a great variety of xenobiotics as well as endogeneous compounds (Coon et al., 1977; Gillette et al., 1974). The hepatic enzyme has been purified to apparent homogeneity as judged by various criteria from rats (Guengerich, 1978; Ryan et al., 1979; West et al., 1979), rabbits (Coon et al., 1978; Imai & Sato, 1974; Johnson & Muller-Eberhard, 1977; Kawalek et al., 1975; Philpot & Arinc, 1976), and mice (Huang et al., 1976). A large body of evidence has been accumulated which suggests that multiple forms of P-450 exist in experimental animals and that some are inducible [for reviews, see Guengerich (1979) and Lu (1979)]. Different animal species appear to contain different subsets of P-450s. This multiplicity appears to be important in the regulation of the types of P-450-mediated reactions carried out in a given individual (Coon et al., 1977).

Wide variation of carcinogen-metabolizing activities attributed to P-450 has been observed in human samples (Harris et al., 1979; Sabadie et al., 1980). Extension of the knowledge of P-450s in humans had been hampered by technical diffi-

† From the Department of Biochemistry and Center in Environmental Toxicology, Vanderbilt University School of Medicine, Nashville, Tennessee 37232. *Received May 2, 1980; revised manuscript received September 2, 1980.* This work was supported in part by Grants ES 01590 and ES 00267 and Contract NCI NO 1 CP 85672 from the U.S. Public Health Service.

* Address correspondence to this author. He is a recipient of Research Career Development Award ES 00041 from the U.S. Public Health Service.

[1] Abbreviations used: P-450, liver microsomal cytochrome P-450; C′, complement; Tris, 2-amino-2-(hydroxymethyl)-1,3-propanediol; EDTA, (ethylenedinitrilo)tetraacetic acid; RIA, competitive radioimmune assay; IgG, immunoglobulin G fraction; PB, phenobarbital; 3MC, 3-methylcholanthrene; BNF, β-naphthoflavone (5,6-benzoflavone); $NaDodSO_4$, sodium dodecyl sulfate; M_r, apparent monomeric molecular weight as determined by $NaDodSO_4$–polyacrylamide gel electrophoresis.

0006-2960/81/0420-2370$01.25/0 © 1981 American Chemical Society

EXHIBIT 16

Biochemistry **1998**, *37*, 9266−9273

Contribution of Domain Interface Residues to the Stability of Antibody C_H3 Domain Homodimers

William Dall'Acqua,[‡] Alexander L. Simon,[‡,§] Michael G. Mulkerrin,[‖] and Paul Carter*[,‡]

Departments of Molecular Oncology and Medicinal & Analytical Chemistry, Genentech Inc., 1 DNA Way, South San Francisco, California 94080

Received February 3, 1998; Revised Manuscript Received April 22, 1998

ABSTRACT: Dimers of C_H3 domains from human IgG_1 were used to study the effect of mutations constructed at a domain−domain interface upon domain dissociation and unfolding, "complex stability". Alanine replacement mutants were constructed on one side of the interface for each of the sixteen interdomain contact residues by using a single-chain C_H3 dimer in which the carboxyl terminus of one domain was joined to the amino terminus of the second domain via a $(G_4S)_4$ linker. Single-chain variants were expressed in *Escherichia coli* grown in a fermentor and recovered in yields of 6−90 mg L^{-1} by immobilized metal affinity chromatography. Guanidine hydrochloride-induced denaturation was used to follow domain dissociation and unfolding. Surprisingly, the linker did not perturb the complex stability for either the wild type or two destabilizing mutants. The C_H3 domain dissociation and unfolding energetics are dominated by six contact residues where corresponding alanine mutations each destabilize the complex by >2.0 kcal mol^{-1}. Five of these residues (T366, L368, F405, Y407, and K409) form a patch at the center of the interface and are located on the two internal antiparallel β-strands. These energetically key residues are surrounded by 10 residues on the two external β-strands whose contribution to complex stability is small (three have a $\Delta\Delta G$ of 1.1−1.3 kcal mol^{-1}) or very small (seven have a $\Delta\Delta G$ of ≤0.7 kcal mol^{-1}). Thus, at the center of the C_H3 structural interface there is a small "functional interface" of residues that make significant contributions to complex stability.

Understanding protein−protein recognition is of fundamental significance as many biological processes depend on the ability of proteins to form specific and stable complexes. Protein−protein contact surfaces have been defined at atomic resolution by structure determination for a rapidly expanding number of protein complexes (reviewed in refs *1*−*4*). Extensive mutational analyses of such protein complexes have identified the residues that make significant energetic contributions to binding. In some cases, the energetically important residues represent only a small subset of the contact residues (*5*, *6*), whereas for others, a large proportion of the contact residues are functionally important (*7*).

The most detailed mutational analyses of protein−protein interactions to date have involved pairs of different proteins that can exist both free in solution and also in a bound state, such as ligand−receptor complexes (*5*, *6*) and antibody−antigen complexes (*7*), "noncompulsory complexes". In contrast, there is a paucity of data for the exceedingly common biological motif of "compulsory complexes" (*8*) in which free monomers are not readily detected. This likely reflects problems of interpreting the effects of mutations made simultaneously on both sides of an interface and the technical difficulty in making replacements on only one surface. For example, coexpression of mutant and wild-type chains typically leads to the formation of parental homodimers as well as the desired heterodimer, thereby confounding subsequent analysis of the mutational effects. Appending one of the chains with a charge tag (*9*, *10*) or each chain with either an epitope or polyhistidine tag (*11*) permits purification of the heterodimer away from the two parental homodimers. Nevertheless, subunit dissociation and exchange may lead to formation of parental homodimers that interfere with interpretation of mutational analysis.

An additional difficulty in functional analysis of domain interfaces of compulsory complexes is that mutations may affect unfolding of domains as well as their dissociation. Close coupling of these processes may confound partitioning of mutational effects between them. "Complex stability" here encompasses effects on both domain dissociation and unfolding of a compulsory complex.

We have extended the study of protein−protein recognition to investigate the effect of mutations constructed on one contact surface of a compulsory complex, the homodimer of the C_H3 domain (hdC_H3) from human IgG_1. The C_H3 homodimer was converted to a single-chain format (scC_H3) analogous to that originally described for single-chain Fv (scFv) fragments (*12*, *13*) by installing a peptide linker for connecting the carboxyl terminus of one domain to the amino terminus of the second domain. The linker was found not to significantly modify the stability of wild-type C_H3 or for two of the most destabilizing C_H3 mutants. This allowed us to adopt the scC_H3 format in analyzing the effects of

* Corresponding author. Telephone: (650) 225-1932. Fax: (650) 225-1716. E-mail: pjc@gene.com.
‡ Department of Molecular Oncology.
§ Present address: Cancer Biology, MSOB 309, Mail Code 5404, Stanford University, Stanford, CA 94305.
‖ Department of Medicinal & Analytical Chemistry.

S0006-2960(98)00270-0 CCC: $15.00 © 1998 American Chemical Society
Published on Web 06/06/1998

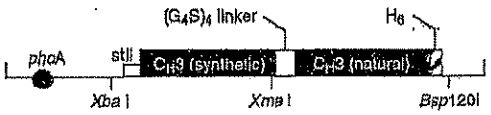

FIGURE 1: Schematic representation of an operon for the expression of scC_H3 in *E. coli* using the phagemid vector pRA4. A synthetic C_H3 gene (*19*) is connected to a natural C_H3 gene (*75*) via a linker encoding the sequence $(G_4S)_4$. The second C_H3 gene is followed by a sequence encoding six histidine residues (H_6) that allows purification by IMAC. The operon is under the transcriptional control of the *E. coli* alkaline phosphatase (*phoA*) promoter (*76*) which can be induced by phosphate starvation. Secretion is directed by the heat stable enterotoxin signal sequence [stII, (*77*)].

mutations installed on only one side of the domain interface upon domain dissociation and unfolding.

The C_H3 interface involves 16 residues located on four antiparallel β-strands that make intermolecular contacts and are buried 1090 Å^2 from each surface (*14*, *15*). These 16 residues were individually replaced with alanine on one side of the interface. Alanine replacements were chosen to minimize unfavorable steric contacts and to avoid imposing new charge interactions or hydrogen bonds from the substituted side chains while minimizing the risk of altering the main chain conformation (*16*−*18*). The contribution of individual residues to complex stability was assessed by comparing guanidine hydrochloride (GuHCl[1])-induced unfolding of wild-type and alanine mutant scC_H3 by far-ultraviolet circular dichroism (far-UV CD) spectroscopy.

MATERIALS AND METHODS

Reagents. Restriction enzymes, Vent DNA polymerase, and other DNA-modifying enzymes were purchased from New England Biolabs, Inc. (Beverly, MA), whereas Sequenase version 2.0 and Muta-Gene kits were obtained from United States Biochemicals (Cleveland, OH) and Bio-Rad (Hercules, CA), respectively. [^{35}S]dATPαS was obtained from Amersham Life Science Inc. (Arlington Heights, IL), and ultrapure guanidine hydrochloride (GuHCl) was purchased from Gibco-BRL. HiTrap nickel nitrilotriacetic acid (Ni^{2+}-NTA) and Superdex 75 columns were obtained from Pharmacia (Uppsala, Sweden). Oligonucleotides were synthesized on an Applied Biosystems (Foster City, CA) model 394 DNA synthesizer.

Single-Chain C_H3 Construction. Phagemid pRA2 contains a dicistronic operon in which C_H3 expressed from a synthetic gene is cosecreted with a second copy of C_H3 expressed from the natural gene as a fusion with M13 gene III (*19*). Phagemid pRA2 was modified to create pRA4 for scC_H3 expression by connecting two C_H3 domains via a $(G_4S)_4$ linker (Figure 1). In addition, the second C_H3 gene was mutagenized to replace M13 gene III with a sequence encoding six histidines to facilitate purification by immobilized metal affinity chromatography (IMAC; *20*). Briefly, the natural C_H3 gene (100 ng) was subjected to a two-step PCR mutagenesis using 50 pmol of the primer 5′-CAAACGAAGGGCCCTTATTAGTGATGGTGATGGTGA-TGTTTACCCGGAGACAGGGAGAGG-3′ (*Bsp*120I site underlined) with successively 50 pmol of the primer 5′-GGCGGAGGTGGTTCTGGCGGTGGCGGATCGG-GGCAGCCCCGAGAACCACAGGTGTACACCCTGCC-CCCATCTCGGGAAG-3′ and 50 pmol of the primer 5′-AAAAAGGGTATCTAGAGGTTGAGGTGATTTTT-CCCTGTCTCCCGGGAAAGGTGGAGGCGGTTCAGG-TGGAGGCGGTTCAGGCGGAGGTGGTT-3′ (underlined sites for *Xba*I and *Xma*I, respectively), each dNTP at 200 μM, 100 mM Tris-HCl (pH 8.3), 500 mM KCl, 1.5 mM $MgCl_2$, 0.01% (w/v) gelatin, and 3 units of Vent DNA polymerase. The sample was incubated at 94 °C for 5 min followed by 30 rounds of thermocycling (94 °C for 1 min, 50 °C for 1 min, and 72 °C for 1 min) using a GeneAmp PCR System 9600 (Perkin-Elmer, Norwalk, CT). The amplified DNA was digested with *Xba*I and *Bsp*120I and cloned into pRA2 (*19*) restricted with the same enzymes to create phagemid pRA3. The scC_H3 expression phagemid, pRA4, was constructed by subcloning the synthetic C_H3 gene as an *Xba*I−*Xma*I fragment into similarly cleaved pRA3. The sequence was verified by dideoxynucleotide sequencing (*21*) using Sequenase version 2.0.

Site-Directed Mutagenesis. Mutants were prepared by site-directed mutagenesis using the method of Kunkel (*22*) in conjunction with a Muta-Gene kit. The oligonucleotides for mutagenesis were designed to replace the chosen wild-type codons in the synthetic C_H3 gene with the alanine codon, GCT. Mutations were constructed using phagemid pRA2 (*19*) modified to contain either synthetic or natural C_H3 and verified by dideoxynucleotide sequencing.

Expression and Purification of C_H3 Variants. Phagemids for the expression of hdC_H3 and scC_H3 variants were transformed into *Escherichia coli* 33B6 (*23*). The C_H3 variants were secreted from corresponding *E. coli* cells cultured for approximately 48 h at 30 °C in an aerated 10 L fermentor (*24*). The cell density at harvest was in the range of 100−150 OD_{550}. The hdC_H3 and scC_H3 variants were purified as described previously (*19*) or below, respectively.

A periplasmic fraction was prepared (*19*) from 100 g of fermentation paste for each scC_H3 variant and dialyzed extensively against 50 mM Tris-HCl (pH 8.0). The dialysate was adjusted to 25 mM imidazole and applied to a 5 mL Ni^{2+}-NTA affinity column. The resin was washed with 20 column volumes of 50 mM Tris-HCl (pH 8.0), and the scC_H3 variants were eluted with a linear gradient of 0 to 500 mM imidazole in 50 mM Tris-HCl (pH 7.5). The purified scC_H3 variants were dialyzed against 50 mM sodium phosphate buffer (pH 7.4) or 10 mM Tris-HCl (pH 8.0) and 10 mM NaCl. The scC_H3 variants were analyzed by size exclusion chromatography on a Superdex 75 column in phosphate-buffered saline.

The purified hdC_H3 and scC_H3 variants were concentrated using Centriprep-10 concentrators (Amicon, Beverley, MA), flash-frozen in liquid nitrogen, and stored at −70 °C. The protein yields were estimated from the absorbance at 280 nm using the extinction coefficients (ϵ_{280}) for the wild-type hdC_H3 and scC_H3 determined by amino acid hydrolysis to be 32 204 and 38 107 cm^{-1} M^{-1}, respectively.

Far-UV CD Spectroscopy. Data were obtained as described by Zhukovsky et al. (*25*) on an AVIV (Lakewood, NJ) 60DS spectropolarimeter. Briefly, spectra for scC_H3 and hdC_H3 variants (25−80 μM) were recorded at 20.0 ± 0.1

[1] Abbreviations: Flk-1, fetal liver kinase 1; GuHCl, guanidine hydrochloride; HEL, hen egg white lysozyme; hdC_H3, homodimer C_H3; IMAC, immobilized metal affinity chromatography; KDR, kinase insert domain-containing receptor; NTA, nitrilotriacetic acid; scC_H3, single-chain C_H3; UV CD, ultraviolet circular dichroism; VEGF, vascular endothelial growth factor; θ_{obs}, ellipticity.

°C in 10 mM Tris-HCl (pH 8.0) and 10 mM NaCl. Data were collected over the wavelength range of 250−200 nm in 0.25 nm intervals in a thermostated circular cuvette with a 0.1 cm path length. The final spectra represent the mean of five far-UV CD scans with an integration time of 2 s per data point. Results are reported as mean residue weight ellipticity (θ_{MRW}, in deg cm^2 dmol^{-1}) calculated using the appropriate mean residue weights for each hdC$_H$3 and scC$_H$3 variant.

Equilibrium Denaturation Assays. Guanidine hydrochloride-induced unfolding of hdC$_H$3 and scC$_H$3 variants was followed by far-UV CD spectroscopy at a wavelength of 225 nm. The C$_H$3 variants (25−30 samples at ~1 mg mL^{-1}) were prepared with varying concentrations of GuHCl (0−8 M) in 50 mM sodium phosphate (pH 7.4) and equilibrated for 24 h at 20.0 ± 0.1 °C prior to data collection. Ellipticity θ_{obs} was measured at a wavelength of 225 nm in circular cuvettes with a 0.1 cm path length. A total of 120 data points were taken in a 2 min trace, and the mean was calculated. The final concentrations of GuHCl in each sample were determined by measurement of the refractive index (*26*).

The ellipticity data were fitted by a nonlinear least-squares method to both two-state (*27*) and three-state (*28*) models of unfolding using KaleidaGraph, version 3.0.8 (Synergy Software, PCS Inc., Reading, PA), taking into account the slopes of the pre- and post-transitional baselines. Virtually identical estimates were obtained using the linear extrapolation method (*29*), as already noted (*25*) (data not shown). Denaturation parameters that were estimated include ΔG_0, the free energy of unfolding in the absence of denaturant, and $D_{50\%}$, the denaturant concentration at which the apparent free energy change of unfolding, ΔG_U, is zero. In addition, estimates were made for m, the slope of ΔG_U versus the denaturant concentration D. The errors associated with $D_{50\%}$ values are commonly less significant than those associated with ΔG_0 values which are extrapolated to 0 M GuHCl (*30*, *31*). Consequently, the difference in the free energy of domain dissociation and unfolding between the wild type and the mutant, $\Delta\Delta G$, is more accurately determined in the transition region, using the following equation:

$$\Delta\Delta G = \langle m \rangle (D_{50\%\,wt} - D_{50\%\,mut}) \qquad (1)$$

where $\langle m \rangle$ is the mean value of m for all of the variants (*25*, *32*). A one-way analysis of variance (ANOVA) was consistent with m being independent of variant except for the F405A/F405′A[2] mutant in hdC$_H$3 and scC$_H$3 formats. The F405A/F405′A mutant was therefore excluded in the calculation of $\langle m \rangle$ (*25*).

Mass Spectrometry. C$_H$3 variants in 50 mM sodium phosphate buffer (pH 7.4) were mass analyzed with a packed capillary liquid chromatography system coupled directly to a PE-Sciex API 3 triple-quadrupole mass spectrometer as described (*33*).

[2] Mutations in C$_H$3 domains are denoted by the amino acid residue and number [Eu numbering scheme of Kabat et al. (*78*)], followed by the replacement amino acid. Mutations constructed in a pair of C$_H$3 domains are separated by a slash with a prime sign used to indicate the residue on the second domain. For example, F405A and F405A/F405′A represent replacements of the phenylalanine at position 405 with alanine on one or both domains, respectively.

Table 1: Expression, Purification, and Mass Analysis of C$_H$3 Variants

C$_H$3 variant	yield (mg L^{-1})	observed mass (Da)	expected mass (Da)[a]
homodimers			
wild-type	310	12 106 ± 2	12 107
F405A/F405′A	20	12 032 ± 1	12 031
Y407A/Y407′A	35	12 015 ± 1	12 015
single chains			
wild-type	18	26 281 ± 1	26 281
Q347A	61	26 222 ± 2	26 224
Y349A	36	26 190 ± 1	26 189
T350A	81	26 252 ± 1	26 251
L351A	41	26 239 ± 1	26 239
T366A	75	26 249 ± 2	26 251
L368A	90	26 239 ± 1	26 239
K370A	72	26 224 ± 1	26 224
K392A	9	26 222 ± 2	26 224
T394A	41	26 249 ± 2	26 251
P395A	52	26 252 ± 3	26 255
V397A	65	26 252 ± 1	26 253
L398A	6	26 240 ± 2	26 239
D399A	10	26 237 ± 1	26 237
F405A	14	26 204 ± 1	26 205
F405A/F405′A	8	26 129 ± 1	26 129
Y407A	37	26 189 ± 2	26 189
Y407A/Y407′A	57	26 097 ± 3	26 097
K409A	8	26 223 ± 2	26 224

[a] By high-resolution mass spectrometry.

RESULTS

Design of scC$_H$3 and Mutational Analysis Strategy. A single-chain form of C$_H$3 was designed by utilizing a flexible linker to span from K453 at the carboxyl terminus of C$_H$3 to G341 at the amino terminus of the partner C$_H$3 domain. Unfortunately, this distance could not be accurately estimated since the 10 carboxyl-terminal residues, S444−K453, are not defined in the original 2.8 Å X-ray crystallographic structure of human IgG$_1$ Fc (*14*) or in a more recent higher-resolution (2.0 Å) structure (M. Ultsch and A. M. de Vos, personal communication). L443, the carboxyl-terminal structurally defined residue, is approximately 37 Å from residue G341 of the partner C$_H$3 domain. scC$_H$3 domains were constructed with a long linker, $(G_4S)_4$, in an attempt to accommodate the uncertainty in the distance to be spanned. The second copy of C$_H$3 was followed by a sequence encoding six histidines to permit purification by IMAC (Figure 1).

The 16 domain interface residues were individually replaced with alanine on one side of the interface, the amino-terminal C$_H$3 domain of scC$_H$3. Mutants with replacements on both sides of the interface, namely, F405A/F405′A and Y407A/Y407′A, together with the wild type were constructed in both hdC$_H$3 and scC$_H$3 formats to assess the effect of the linker upon complex stability.

Expression and Purification of hdC$_H$3 and scC$_H$3 Variants. All C$_H$3 variants were secreted from *E. coli* grown to high cell density in a fermentor. The scC$_H$3 variants were purified by IMAC and eluted as a single peak at ~150 mM imidazole (not shown), whereas the hdC$_H$3 variants were recovered by chromatography using ion exchange and ABx resins as described previously (*19*). Sufficient protein was recovered for all C$_H$3 variants to support further analysis, although the recovered yield varied from 35−310 to 6−90 mg L^{-1} for hdC$_H$3 and scC$_H$3 variants, respectively (Table 1). The molecular masses of all C$_H$3 variants determined by high-

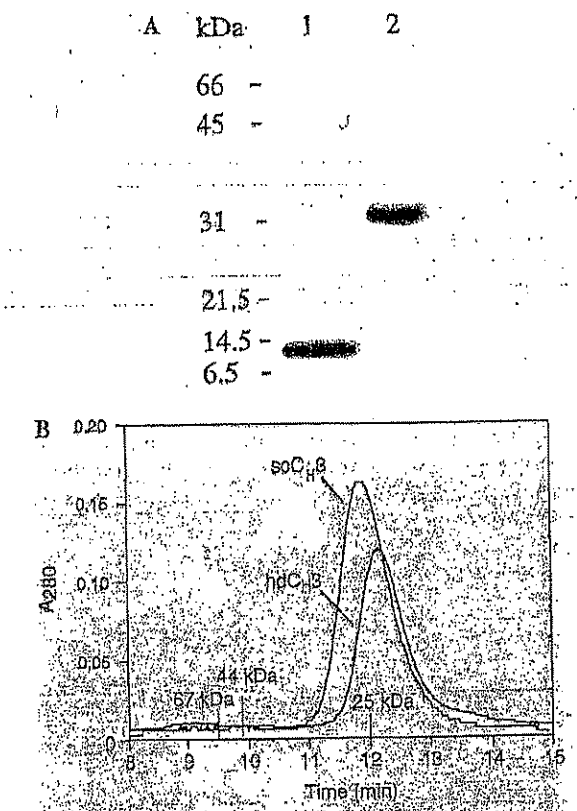

FIGURE 2: Purification of wild-type hdC_H3 and scC_H3 variants. (A) SDS–PAGE analysis using 4 to 20% acrylamide (Novex, San Diego, CA) after staining with Coomassie Blue: lane 1, purified wild-type scC_H3; and lane 2, purified wild-type hdC_H3. (B) Size exclusion chromatography of wild-type hdC_H3 and scC_H3 variants. The molecular mass standards elute as follows: bovine chymotrypsinogen A, 25 kDa, 12.0 min; chicken ovalbumin, 44 kDa, 9.9 min; and bovine serum albumin, 67 kDa, 9.4 min.

resolution electrospray mass spectrometry are consistent with those expected (Table 1).

Wild-type scC_H3 and hdC_H3 each migrate as a single major band when analyzed by SDS–PAGE with apparent molecular masses of 31 and 12 kDa, respectively (Figure 2A). Wild-type scC_H3 has an electrophoretic mobility lower than expected from its molecular mass (27 kDa), which may reflect the presence of the hexahistidine tag. Similar results were obtained with all other scC_H3 and hdC_H3 variants (not shown). Size exclusion chromatographs of wild-type (Figure 2B) and mutant scC_H3 (not shown) are consistent with the presence of the anticipated ~25 kDa monomer with no evidence for dimers or higher-order polymers.

Far-UV CD Spectroscopy and Equilibrium Denaturation Assays for C_H3 Variants. The wild-type scC_H3 fragment gave rise to a far-UV CD spectrum that is indistinguishable from that of the corresponding hdC_H3 (Figure 3), including a minimum at a wavelength of 225 nm characteristic of β-sheet structures (*34*). This wavelength was chosen for following the GuHCl-induced unfolding and dissociation of C_H3 variants. Unfolding and dissociation is fully reversible as judged by the complete recovery of original ellipticity upon dilution of the denatured samples as described (*25*, *35*). In contrast, thermal unfolding of hdC_H3 is not fully reversible and aggregation occurs at elevated temperatures (*19*).

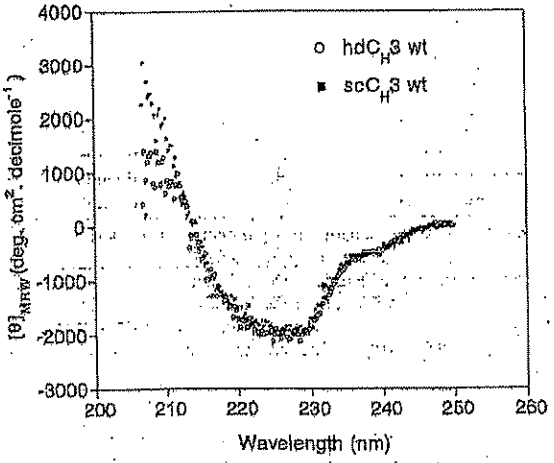

FIGURE 3: Far-UV CD spectra of wild-type scC_H3 and hdC_H3 variants recorded at 20.0 ± 0.1 °C in 10 mM Tris-HCl (pH 8.0) and 10 mM NaCl.

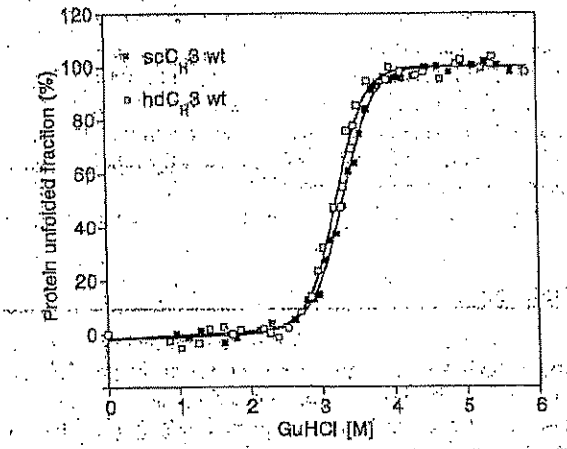

FIGURE 4: Equilibration denaturation profiles of wild-type scC_H3 and hdC_H3 recorded in 50 mM sodium phosphate (pH 7.4) at 20.0 ± 0.1 °C in the presence of varying amounts of GuHCl. Data were fitted using a nonlinear least-squares method to a two-state model (*27*).

GuHCl-induced denaturation data were analyzed by the nonlinear least-squares method of Santoro and Bolen (*27*) to estimate ΔG_0. All data were found to fit better to two-state than to three-state models as judged by lower χ^2 values (not shown). In addition, the transitions observed were continuous, an indication of rapid equilibration between two states (*27*) consistent with close coupling between dissociation of C_H3 domains and their unfolding.

Validation of the Use of the Linker. Wild-type C_H3 in single-chain and homodimer formats show identical stability profiles (Figure 4) and fitted parameters (Table 2) following GuHCl-induced denaturation, indicating that the linker does not significantly modify complex stability. Variants F405A/F405′A and Y407A/Y407′A containing destabilizing mutations on both sides of the C_H3 interface also gave very similar denaturation profiles and parameters in hdC_H3 and scC_H3 formats (Table 2). Taken together, these data support the use of the scC_H3 format in analyzing the effect of alanine scanning mutations constructed on one side of the C_H3 domain interface.

Table 2: Equilibrium Denaturation Parameters for hdC_H3 and scC_H3 Variants[a]

C_H3 variant	format	ΔG_0[b] (kcal mol^{-1})	$D_{50\%}$[c] (M)	m[d] (kcal mol^{-2} L)	$\Delta\Delta G$[e] (kcal mol^{-1})
wild-type	hd	9.1 ± 0.4	3.19 ± 0.14	2.92 ± 0.24	(0)
wild-type	sc	9.1 ± 0.3	3.25 ± 0.08	2.80 ± 0.06	(0)
F405A/F405′A	hd	1.1 ± 0.2	1.20 ± 0.02	0.92 ± 0.22	6.4
F405A/F405′A	sc	1.2 ± 0.3	1.05 ± 0.17	1.15 ± 0.07	6.1
Y407A/Y407′A	hd	4.9 ± 0.4	1.66 ± 0.08	2.81 ± 0.06	4.0
Y407A/Y407′A	sc	4.3 ± 0.4	1.74 ± 0.15	2.52 ± 0.11	4.0

[a] Estimates of the denaturation parameters were performed in duplicate or triplicate. Errors shown are twice the standard deviation of the measurements. [b] ΔG_0, free energy of unfolding in the absence of the denaturant estimated by nonlinear least-squares fitting of the raw data to a two-state model for unfolding. [c] $D_{50\%}$, denaturant concentration at which the apparent free energy of unfolding $\Delta G_u = 0$ kcal mol^{-1}. [d] m, slope of ΔG_u vs D. [e] $\Delta\Delta G$, difference in the free energy of unfolding between wild-type scC_H3 and hdC_H3 and variants in the same format. $\Delta\Delta G$ values were calculated from eq 1 using 2.65 kcal mol^{-1} (SD of 0.18 kcal mol^{-1}), the mean value of m for all proteins, excluding hdC_H3 F405A/F405′A and scC_H3 F405A/F405′A. The standard deviation for $\Delta\Delta G$ values is 0.1–0.15 kcal mol^{-1} except for that for hdC_H3 F405A/F405′A (0.25 kcal mol^{-1}).

Alanine Scanning Mutagenesis of the C_H3 Domain Interface. The largest reductions in complex stability ($\Delta\Delta G$ > 2.0 kcal mol^{-1}) occurred on alanine substitution of residues T366, L368, P395, F405, Y407, and K409. Significant destabilizing effects ($\Delta\Delta G$ = 1.0–1.3 kcal mol^{-1}) were also seen on substitution of residues Q347, L351, and K370. Alanine replacements of the seven other interface residues (Y349, T350, K392, T394, V397, L398, and D399) had small or insignificant effects upon complex stability ($\Delta\Delta G \leq 0.7$ kcal mol^{-1}). These data from alanine scanning mutagenesis indicate that residues in the two internal antiparallel β-strands contribute significantly more to complex stability than residues in the two external antiparallel β-strands (Figure 5).

DISCUSSION

Single-Chain Strategy. A mutational analysis of the human IgG_1 C_H3 domain was undertaken to quantify the contribution of interdomain contact residues to domain dissociation and unfolding of this compulsory complex. A scC_H3 dimer was constructed by joining the carboxyl terminus of one domain to the amino terminus of the second domain via a 20-residue linker. This permitted mutations to be constructed on one side of the interface, thereby avoiding the complication of attempting to interpret mutations constructed simultaneously on both sides of the interface.

The linker was anticipated to stabilize the C_H3 dimer by virtue of increasing the local concentration of monomers. Such stabilization has been previously demonstrated for analogous linkers in a scFv fragment (*36*) and a single-chain version of the homodimeric bacteriophage P22 Arc repressor (*37*). Surprisingly, the linker did not significantly affect the free energy change upon domain dissociation and unfolding for wild-type C_H3 and two destabilized mutants, F405A/F405′A and Y407A/Y407′A (Table 2). The $(G_4S)_4$ linker may be sufficiently long and flexible that the increased stability anticipated from a high local concentration of monomers (*37*) is lost. Alternatively, the concentration of C_H3 variants (1 mg mL^{-1}) used for denaturation experiments may be too high to observe the effects due to the covalent linkage. Wild-type C_H3 in homodimeric and single-chain formats exhibits indistinguishable CD spectra (Figure 3), indicating no gross perturbation of the secondary structure (*38*) or of the β-sheets packing (*39*, *40*). Taken together, these data suggest that scC_H3 is a good substitute for heterodimeric C_H3 for analyzing the effect of mutations on only one side of the domain interface.

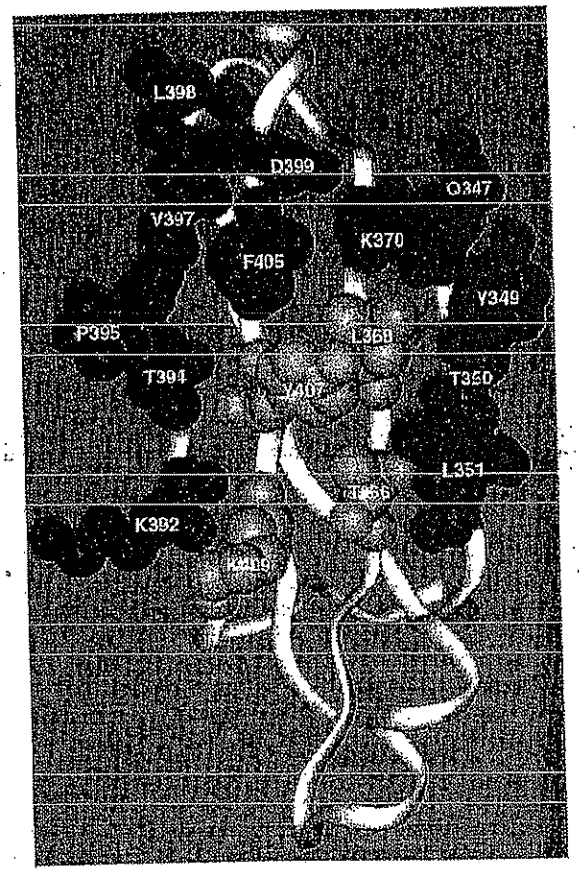

FIGURE 5: Space-filling model of the surface of C_H3 in contact in the C_H3–C_H3 complex based upon the human IgG_1 structure of Deisenhofer (*14*). Residues are color-coded according to the loss of free energy of stabilization upon alanine substitution: red, ≥2.5 kcal mol^{-1}; yellow, 2.0–2.4 kcal mol^{-1}; and blue, <1.5 kcal mol^{-1}.

No free monomer has been detected in C_H3 (pFc′) preparations at concentrations as low as 10^{-10} M (*41*). This is consistent with C_H3 dimers having a dissociation constant (K_D) of $<10^{-10}$ M (*42*) corresponding to a free energy change upon dissociation of >13 kcal mol^{-1} calculated using the well-known relationship

$$\Delta G = RT \ln K_D \qquad (2)$$

where R is the gas constant and T the absolute temperature (293 K). In contrast, the free energy change upon hdC_H3 dissociation and unfolding was estimated to be 9.1 kcal mol^{-1} (Table 2). These data are consistent with the C_H3 domains being stabilized by their association.

A concern with the interdomain linker is that it might promote C_H3 dimerization or multimerization as shown with single-chain Fv fragments, particularly with linkers of 10 or fewer residues (*43*−*45*). The scC_H3 constructed with a 20-residue linker is monomeric as judged by size exclusion chromatography, with no evidence for multimerization (Figure 2B). In contrast, size exclusion chromatography of scC_H3 constructed with a shorter linker, $(G_4S)_3$, is consistent with a monomer−dimer equilibrium (data not shown).

Interpretation of the Denaturation Parameters. Stabilization of C_H3 dimers is largely mediated by six of the 16 residues tested: T366, L368, P395, F405, Y407, and K409 (Figure 5). Residues T366 and Y407 form a hydrogen bond and represent the principal intermolecular and intramolecular contact with each other. Alanine substitution of Y407 and T366 reduces the complex stability by 2.3 and 2.1 kcal mol^{-1}, respectively. This loss in stability is consistent with the 1.0−2.5 kcal mol^{-1} reduction in free energy seen on replacing hydrogen-bonding residues in other proteins where both donor and acceptor residues are uncharged (*46*−*49*). Unfortunately, the exact strength of hydrogen bonds cannot be accurately determined from such single-mutation data since other interactions (van der Waals and hydrophobic) that may contribute to stabilization of the interface are concomitantly perturbed (*32*, *50*, *51*). Furthermore, the introduction of cavity-creating mutations might be followed by compensatory structural rearrangements (*52*−*54*) or solvent reorganization (*55*). A more accurate estimation of strength of the hydrogen bond between residues T366 and Y407′ awaits the construction of additional mutations and structural analysis of the corresponding mutant proteins.

Residue K409 forms a hydrogen bond with residue D399 on the partner C_H3 domain (*14*, *15*). Truncation of the K409 side chain to alanine significantly decreases complex stability ($\Delta\Delta G$ = 2.4 kcal mol^{-1}), whereas pruning the D399 side chain results in only a small reduction in stability ($\Delta\Delta G$ = 0.7 kcal mol^{-1}) (Table 3). There are numerous possible explanations for the asymmetry of these mutational effects at residues K409 and D399, including the possibility that these residues are not the major energetic contacts with each other. For example, the near functional silence of D399 may reflect that the fact that the cost of desolvating this residue is comparable to the energy gained through intermolecular contact with K409. The release of water molecules is not a major contributor to the stabilization of some protein−protein complexes (*56*, *57*). Alternatively, the larger effect observed for substitution of residue K409 than for D399, its hydrogen bond partner, can be explained by an effect of K409 on folding of the corresponding domain.

Residues L368 and F405 form intermolecular and intramolecular contacts through van der Waals interactions only. The large decrease in stability upon substitution of these residues with alanine likely reflects the contribution of the hydrophobic effect and of van der Waals contacts as well as probable solvent and protein structure rearrangements. The strength of the van der Waals contacts has been estimated to be approximately 0.5 kcal mol^{-1} (*49*, *55*).

Table 3: Equilibrium Denaturation Parameters for scC_H3 Alanine Variants[a]

C_H3 variant	ΔG_0 (kcal mol^{-1})	$D_{50\%}$ (M)	m (kcal mol^{-2} L)	$\Delta\Delta G^b$ (kcal mol^{-1})
Q347A	8.4 ± 0.4	2.86 ± 0.06	2.93 ± 0.20	1.1
Y349A	8.5 ± 0.2	3.00 ± 0.01	2.83 ± 0.06	0.7
T350A	8.8 ± 0.1	3.21 ± 0.01	2.76 ± 0.06	0.1
L351A	7.0 ± 0.4	2.76 ± 0.02	2.52 ± 0.18	1.3
T366A	6.3 ± 0.2	2.38 ± 0.02	2.65 ± 0.11	2.3
L368A	6.1 ± 0.3	2.40 ± 0.04	2.52 ± 0.20	2.2
K370A	6.9 ± 0.3	2.83 ± 0.08	2.45 ± 0.12	1.1
K392A	8.5 ± 0.3	3.11 ± 0.19	2.75 ± 0.04	0.4
T394A	8.1 ± 0.1	3.02 ± 0.01	2.67 ± 0.04	0.6
P395A	5.3 ± 0.4	2.08 ± 0.03	2.62 ± 0.11	3.2
V397A	7.7 ± 0.3	3.02 ± 0.01	2.57 ± 0.09	0.6
L398A	8.2 ± 0.3	3.23 ± 0.04	2.55 ± 0.08	0.1
D399A	8.2 ± 0.3	2.99 ± 0.02	2.72 ± 0.06	0.7
F405A	5.8 ± 0.1	2.32 ± 0.03	2.50 ± 0.07	2.5
Y407A	6.6 ± 0.4	2.49 ± 0.02	2.65 ± 0.16	2.1
K409A	5.2 ± 0.1	2.37 ± 0.11	2.21 ± 0.04	2.4

[a] Details as described in Table 2. [b] The standard deviation for $\Delta\Delta G$ values was 0.1−0.15 kcal mol^{-1} except for that for K392A (0.25 kcal mol^{-1}).

The most destabilizing mutation ($\Delta\Delta G$ = 3.2 kcal mol^{-1}), P395A, is located in a peripheral β-strand. Replacement of this proline residue likely perturbs the local backbone conformation, thereby indirectly affecting intermolecular interactions involving neighboring residues. Cis to trans isomerization of the peptide bond at P395 is not a plausible hypothesis for explaining the effects of the P395A replacement since this residue in wild-type C_H3 is in the trans rather than in the cis conformation (M. Ultsch and A. M. de Vos, personal communication). Substitution of proline residues in proteins with smaller amino acids is believed to be destabilizing through local conformational effects (*58*−*60*) or through stabilization of the unfolded state (*61*). A proline to serine substitution in nucleoside diphosphate kinase compromised the ability of the isolated subunits to associate into a hexamer (*60*). This effect was attributed to a change in the flexibility of the proline-containing loop constituting the domain−domain interface.

The m parameter reflects the difference between the solvent-exposed nonpolar surface area of the denatured and native states of proteins and/or the cooperativity of protein unfolding (*29*, *62*). Thus, the significant change in m for the F405A/F405′A double mutant may reflect the presence of equilibrium intermediates during unfolding or changes in the solvation properties of the denatured state.

Additivity of Mutational Effects. The reduction in stability for the double mutant, Y407A/Y407′A scC_H3 ($\Delta\Delta G$ = 4.0 kcal mol^{-1}), approximately equals the sum of stability reductions of the constituent single mutants Y407A and Y407′A ($\Delta\Delta G$ = 2.1 kcal mol^{-1}). This functional additivity (*63*) is consistent with Y407A and Y407′A having only local effects that are independent of each other. Residues Y407 and Y407′ are ~5 Å apart at the interface and do not form any intermolecular contacts (*14*). In contrast, the double mutant F405A/F405′A scC_H3 is destabilized by 1.1 kcal mol^{-1} more than predicted by adding the $\Delta\Delta G$ terms for the component single mutants. Thus, residues F405 and F405′ are energetically coupled although separated by >12 Å. Nonadditivity of distant mutations has been observed in several other systems, including barnase−barstar (*64*), sta-

phylococcal nuclease (*65*), human hemoglobin (*66*), and an antibody−anti-idiotype (*49*). Several possible explanations for long distance nonadditivity have been proposed (*67*), including solvent rearrangements, as described at the domain interface for a complex between a mutant antibody and chicken lysozyme (*55*, *68*).

Relationship between Structural and Functional Interface. A priori, the binding interaction between two proteins might be mediated primarily by a few strong interactions involving a small subset of interface residues or through a larger number of contact residues each making small contributions. In the case of the scC_H3 compulsory complex, six of the 16 interface residues account for the majority of the energy of stabilization. The residues most critical for scC_H3 stabilization are located on the two interior β-strands, forming a patch at the center of the interface (Figure 5). P395 notwithstanding, residues at the periphery make very little net contribution to the free energy of scC_H3 stabilization. Thus, scC_H3 is stabilized by an "energetic interface" between C_H3 domains located at the heart of a larger "structural interface".

Small energetic interfaces have been observed previously for the noncompulsory complexes between human growth hormone and its receptor (*5*, *69*) and for vascular endothelial growth factor (VEGF) and its KDR and Flk-1 receptors (*6*). A few strong interactions at the center of an interface also dominate the energetics of binding of the complex between hen egg white lysozyme and the monoclonal antibody D1.3 (*7*). In contrast, the majority of the contact residues play a significant role in binding (> 1.5 kcal mol^{-1}) for an antibody−anti-idiotype complex (*7*).

Nature of the Functional Interface. Mutational analysis of the compulsory complex of scC_H3 indicates that residues making major contributions to domain stability and/or association have side chains that are hydrophobic (F405 and L368), polar (T366 and Y407), or charged (K409). Similarly, both polar and nonpolar residues play an important energetic role in association of the noncompulsory complexes of chicken lysozyme with a cognate monoclonal antibody (*7*) and of VEGF with its KDR receptor (*6*). In contrast, the energetics of human growth hormone associating with its receptor relies primarily upon hydrophobic residues (*5*). Thus, there is much variation in the chemical nature of the energetic interface residues among compulsory and noncompulsory complexes studied to date.

The free energy of the C_H3-C_H3 complex stabilization appears to arise from only half of the antiparallel β-strand constituting the interface. Several different models of β-sheet packing have been described, including aligned (*70*), three-layer (*71*), and intercalated (*15*). Whether the main features of the energetic map we describe here are to be generalized for those different kinds of β-sheets-involving interfaces is still to be determined. Since the interior of many monomeric proteins is formed by β-sheet packing, the quantitative information we gained from this study is also highly relevant to the issue of protein stabilization.

Summary. We have shown that approximately one-third of the contact side chains at the human IgG1 C_H3 domain interface can account for the majority of contributions to domain folding and association. These residues cluster near the center of the structural interface. This study will help us to progress from purely anatomical descriptions of protein−protein interfaces such as their sizes, the identity of contact residues, the amount of buried surface areas, the number of hydrogen bonds, and van der Waals interactions (*72*−*74*) to a detailed understanding of how these structural features contribute to the affinity and specificity of the binding reactions. To our knowledge, this is the first extensive mutational analysis of the domain interface of a compulsory protein complex.

ACKNOWLEDGMENT

We thank Bart de Vos and Mark Ultsch for sharing unpublished X-ray crystallographic coordinates of a human IgG_1 Fc, Mark Vasser, Parkash Jhurani, Peter Ng, and Kristina Azizian for synthetic oligonucleotides, Brad Snedecor and Han Chen for *E. coli* fermentations, Jim Bourell for mass spectrometry of the proteins, Allan Padua for amino acid hydrolysis analysis, and Bob Kelley for helpful discussions and review of the manuscript.

REFERENCES

1. Davies, D. R., Padlan, E., and Sheriff, S. (1990) *Annu. Rev. Biochem. 59*, 439−473.
2. Marluzza, R. A., and Poljak, R. J. (1993) *Curr. Opin. Immunol. 5*, 50−55.
3. Webster, D. M., Henry, A. H., and Rees, A. R. (1994) *Curr. Opin. Struct. Biol. 4*, 123−129.
4. Braden, B. C., and Poljak, R. J. (1995) *FASEB J. 9*, 9−16.
5. Clackson, T., and Wells, J. A. (1995) *Science 267*, 383−386.
6. Muller, Y. A., Li, B., Christinger, H. W., Wells, J. A., Cunningham, B. C., and de Vos, A. M. (1997) *Proc. Natl. Acad. Sci. U.S.A. 94*, 7192−7197.
7. Dall'Acqua, W., Goldman, E. R., Eisenstein, E., and Marluzza, R. A. (1996) *Biochemistry 35*, 9667−9676.
8. Goodsell, D. S., and Olson, A. J. (1993) *Trends Biochem. Sci. 18*, 65−68.
9. Deonarain, M. P., Scrutton, N. S., and Perham, R. N. (1992) *Biochemistry 31*, 1491−1497.
10. Deonarain, M. P., Scrutton, N. S., and Perham, R. N. (1992) *Biochemistry 31*, 1498−1504.
11. Elsevier, J. P., Wells, L., Quimby, B. B., and Fridovich-Keil, J. L. (1996) *Proc. Natl. Acad. Sci. U.S.A. 93*, 7166−7171.
12. Bird, R. E., Hardman, K. D., Jacobson, J. W., Johnson, S., Kaufman, B. M., Lee, S. M., Lee, T., Pope, S. H., Riordan, G. S., and Whitlow, M. (1988) *Science 242*, 423−426.
13. Huston, J. S., Levinson, D., Mudgett-Hunter, M., Tai, M. S., Novotny, J., Margolies, M. N., Ridge, R. J., Bruccoleri, R. E., Haber, E., and Crea, R. (1988) *Proc. Natl. Acad. Sci. U.S.A. 85*, 5879−5883.
14. Deisenhofer, J. (1981) *Biochemistry 20*, 2361−2370.
15. Miller, S. (1990) *J. Mol. Biol. 216*, 965−973.
16. Carter, P., and Wells, J. A. (1988) *Nature 332*, 564−568.
17. Duncan, A. R., and Winter, G. (1988) *Nature 332*, 563−564.
18. Cunningham, B. C., and Wells, J. A. (1989) *Science 244*, 1081−1085.
19. Atwell, S., Ridgway, J. B. B., Wells, J. A., and Carter, P. (1997) *J. Mol. Biol. 270*, 26−35.
20. Hochuli, E. (1988) *J. Chromatogr. 444*, 293−302.
21. Sanger, F., Nicklen, S., and Coulson, A. R. (1977) *Proc. Natl. Acad. Sci. U.S.A. 74*, 5463−5467.
22. Kunkel, T. A., Roberts, J. D., and Zakour, R. A. (1987) *Methods Enzymol. 154*, 367−382.
23. Rodrigues, M. L., Presta, L. G., Kotts, C. E., Wirth, C., Mordenti, J., Osaka, G., Wong, W. L. T., Nuijens, A., Blackburn, B., and Carter, P. (1995) *Cancer Res. 55*, 63−70.
24. Carter, P., Kelley, R. F., Rodrigues, M. L., Snedecor, B., Covarrubias, M., Velligan, M. D., Wong, W. L. T., Rowland, A. M., Kotts, C. E., Carver, M. E., Yang, M., Bourell, J. H., Shephard, H. M., and Henner, D. (1992) *Bio/Technology 10*, 163−168.
25. Zhukovsky, E. A., Mulkerrin, M. G., and Presta, L. G. (1994) *Biochemistry 33*, 9856−9864.

26. Nozaki, Y. (1972) *Methods Enzymol. 26*, 43−50.
27. Santoro, M. M., and Bolen, D. W. (1988) *Biochemistry 27*, 8063−8068.
28. Barrick, D., and Baldwin, R. L. (1993) *Biochemistry 32*, 3790−3796.
29. Greene, R. F., and Pace, C. N. (1974) *J. Biol. Chem. 249*, 5388−5393.
30. Kellis, J. T., Jr., Nyberg, K., and Fersht, A. R. (1989) *Biochemistry 28*, 4914−4922.
31. Horovitz, A., Matthews, J. M., and Fersht, A. R. (1992) *J. Mol. Biol. 227*, 560−568.
32. Serrano, L., Horovitz, A., Avron, B., Bycroft, M., and Fersht, A. R. (1990) *Biochemistry 29*, 9343−9352.
33. Bourell, J. H., Clauser, K. P., Kelley, R., Carter, P., and Stults, J. T. (1994) *Anal. Chem. 66*, 2088−2095.
34. Venyaminov, S. Y., and Yang, J. S. (1996) in *Circular Dichroism and the Conformational Analysis of Biomolecules*, pp 69−107, Plenum Press, New York.
35. Missiakas, D., Betton, J. M., Minard, P., and Yon, J. M. (1990) *Biochemistry 29*, 8683−8689.
36. Glockshuber, R., Malia, M., Pfitzinger, I., and Pluckthun, A. A. (1990) *Biochemistry 29*, 1362−1367.
37. Robinson, C. R., and Sauer, R. T. (1996) *Biochemistry 35*, 13878−13884.
38. Provencher, S. W., and Glockner, J. (1981) *Biochemistry 20*, 33−37.
39. Manning, M. C., and Woody, R. W. (1987) *Biopolymers 26*, 1731−1752.
40. Manning, M. C., Illangasekare, M., and Woody, R. W. (1988) *Biophys. Chem. 31*, 77−86.
41. Ellerson, J. R., Yasmeen, D., Painter, R. H., and Dorrington, K. J. (1976) *J. Immunol. 116*, 510−517.
42. Schiffer, M., Chang, C. H., Naik, V. M., and Stevens, F. J. (1988) *J. Mol. Biol. 203*, 799−802.
43. Holliger, P., Prospero, T., and Winter, G. (1993) *Proc. Natl. Acad. Sci. U.S.A. 90*, 6444−6448.
44. Whitlow, M., Filpula, D., Rollence, M. L., Feng, S. L., and Wood, J. F. (1994) *Protein Eng. 7*, 1017−1026.
45. Desplancq, D., King, D. J., Lawson, A. D. G., and Mountain, A. (1994) *Protein Eng. 7*, 1027−1033.
46. Fersht, A. R., Shi, J., Knill-Jones, J., Lowe, D. M., Wilkinson, A. J., Blow, D. M., Brick, P., Carter, P., Waye, M. M. Y., and Winter, G. (1985) *Nature 314*, 235−238.
47. Street, I. P., Armstrong, C. R., and Withers, S. G. (1986) *Biochemistry 25*, 6021−6027.
48. Shirley, B. A., Stanssens, P., Hahn, U., and Pace, C. N. (1992) *Biochemistry 31*, 725−732.
49. Goldman, E. R., Dall'Acqua, W., Braden, B. C., and Mariuzza, R. A. (1997) *Biochemistry 36*, 49−56.
50. Ackers, G. K., and Smith, F. R. (1985) *Annu. Rev. Biochem. 54*, 597−629.
51. Fersht, A. R. (1988) *Biochemistry 27*, 1577−1580.
52. Eriksson, A. E., Baase, W. A., Zhang, X. J., Heinz, D. W., Blaber, M., Baldwin, E. P., and Matthews, B. W. (1992) *Science 255*, 178−183.
53. Rashin, A. A., Rashin, B. H., Rashin, A., and Abagyan, R. (1997) *Protein Sci. 6*, 2143−2158.
54. Atwell, S., Ultsch, M., de Vos, A. M., and Wells, J. A. (1997) *Science 278*, 1125−1128.
55. Ysern, X., Fields, B. A., Bhat, T. N., Goldbaum, F. A., Dall'Acqua, W., Schwartz, F. P., Poljak, R. J., and Mariuzza, R. A. (1994) *J. Mol. Biol. 238*, 496−500.
56. Ross, P. D., and Subramanian, S. (1981) *Biochemistry 20*, 3096−3102.
57. Bhat, T. N., Bentley, G. A., Boulot, G., Greene, M. I., Tello, D., Dall'Acqua, W., Souchon, H., Schwartz, F. P., Mariuzza, R. A., and Poljak, R. J. (1994) *Proc. Natl. Acad. Sci. U.S.A. 91*, 1089−1093.
58. Koshy, T. I., Luntz, T. L., Schejter, A., and Margoliash, E. (1990) *Proc. Natl. Acad. Sci. U.S.A. 87*, 8697−8701.
59. Schejter, A., Luntz, T. L., Koshy, T. I., and Margoliash, E. (1992) *Biochemistry 31*, 8336−8343.
60. Lascu, I., Deville-Bonne, D., Glaser, P., and Veron, M. (1993) *J. Biol. Chem. 268*, 20268−20275.
61. Alber, T. (1989) *Annu. Rev. Biochem. 58*, 765−798.
62. Shortle, D., and Meeker, A. K. (1986) *Proteins: Struct., Funct., Genet. 1*, 81−89.
63. Wells, J. A. (1991) *Methods Enzymol. 202*, 390−414.
64. Schreiber, G., and Fersht, A. R. (1995) *J. Mol. Biol. 248*, 478−486.
65. Green, S. M., and Shortle, D. (1993) *Biochemistry 32*, 10131−10139.
66. Speros, P. C., LiCata, V. J., Yontani, T., and Ackers, G. K. (1991) *Biochemistry 30*, 7254−7262.
67. LiCata, V. J., and Ackers, G. K. (1995) *Biochemistry 34*, 3133−3139.
68. Fields, B. A., Goldbaum, F. A., Dall'Acqua, W., Malchiodi, E. L., Cauerhff, A., Schwartz, F. P., Ysern, X., Poljak, R. J., and Mariuzza, R. A. (1996) *Biochemistry 35*, 15494−15503.
69. Cunningham, B. C., and Wells, J. A. (1993) *J. Mol. Biol. 234*, 554−563.
70. Chothia, C., and Janin, J. (1981) *Proc. Natl. Acad. Sci. U.S.A. 78*, 4146−4150.
71. Chothia, C., Novotny, J., Bruccoleri, R., and Karplus, M. (1985) *J. Mol. Biol. 186*, 651−663.
72. Janin, J., and Chothia, C. (1990) *J. Biol. Chem. 265*, 16027−16030.
73. Wilson, I. A., and Stanfield, R. L. (1993) *Curr. Opin. Struct. Biol. 3*, 113−118.
74. Davies, D. R., and Cohen, G. H. (1996) *Proc. Natl. Acad. Sci. U.S.A. 93*, 7−12.
75. Ellison, J. W., Berson, B. J., and Hood, L. E. (1982) *Nucleic Acids Res. 10*, 4071−4079.
76. Chang, C. N., Kuang, W. J., and Chen, E. Y. (1986) *Gene 44*, 121−125.
77. Picken, R. N., Mazaitis, A. J., Maas, W. K., Rey, M., and Heyneker, H. (1983) *Infect. Immun. 42*, 269−275.
78. Kabat, E. A., Wu, T. T., Perry, H. M., Gottesman, K. S., and Foeller, C. (1991) *Sequences of Proteins of Immunological Interest*, 5th ed., Vol. 1, pp 688−696, National Institutes of Health, Bethesda, MD.

BI9802701

EXHIBIT 17

THIS EXHIBIT HAS BEEN REDACTED IN ITS ENTIRETY

EXHIBIT 18

THIS EXHIBIT HAS BEEN REDACTED IN ITS ENTIRETY